American Journal of Science

THE EVOLUTION OF VOLCANO-HOSTED GEOTHERMAL SYSTEMS BASED ON DEEP WELLS FROM KARAHA–TELAGA BODAS, INDONESIA

JOSEPH N. MOORE*, RICHARD G. ALLIS**, MICHAL NEMČOK*,
THOMAS S. POWELL***, CAROL J. BRUTON§, PHILIP E. WANNAMAKER*,
IMAM B. RAHARJO§§ and DAVID I. NORMAN§§§

ABSTRACT. Temperature and pressure surveys, fluid samples, and petrologic analyses of rock samples from deep drill holes at the Karaha - Telaga Bodas geothermal field on the volcanic ridge extending northward from Galunggung Volcano, West Java, have provided a unique opportunity to characterize the evolution of an active volcano-hosted geothermal system. Wells up to 3 km in depth have encountered temperatures as high as 353°C and a weakly altered granodiorite that intruded to within 2 to 3 km of the surface. The intrusion is shallowest beneath the southern end of the field where an acid lake overlies a nearly vertical low resistivity structure (<10 ohm-m) defined by magnetotelluric measurements. This structure is interpreted to represent a vapor-dominated chimney that provides a pathway to the surface for magmatic gases.

Four distinct hydrothermal mineral assemblages document the evolution of the geothermal system and the transition from liquid- to vapor-dominated conditions. The earliest assemblage represents the initial liquid-dominated system generated during emplacement of the granodiorite between 5910 ± 76 and 4200 ± 150 y BP. Tourmaline, biotite, actinolite, epidote and clay minerals were deposited contemporaneously at progressively greater distances from the intrusive contact (assemblage 1). At 4200 ± 150 y BP, flank collapse and the formation of the volcano's crater, Kawah Galunggung, resulted in catastrophic decompression and boiling of the hydrothermal fluids. This event initiated development of the modern vapor-dominated regime. Chalcedony and then quartz were deposited as the early low salinity liquids boiled (assemblage 2). Both vapor- and liquid-rich fluid inclusions were trapped in the quartz crystals. Liquid-rich fluid inclusions from the southern part of the field record salinities ranging from 0 to 26 weight percent $NaCl-CaCl_2$ equivalent and locally contain fluorite daughter crystals. We suggest, based on temperature-salinity relationships and evidence of boiling, that these fluids were progressively concentrated as steam was lost from the system. However, mixing with fluids derived from the underlying intrusion or generated during the formation of acid SO_4 water on the vapor-dominated chimney margins could have contributed to the observed salinities. As pressures declined, CO_2– and SO_4-rich steam-heated water drained downward, depositing anhydrite and calcite (assemblage 3) in the fractures, limiting further recharge. Fluid inclusions with salinities up to 31 weight percent NaCl equivalent were trapped in these minerals as the descending water vaporized. The final assemblage is represented by precipitates of NaCl, KCl and $FeCl_x$ deposited on rock surfaces in portions of the vapor-dominated zone that boiled dry. Vapor-dominated conditions extend over a distance of at least 10

---

*Energy & Geoscience Institute, 423 Wakara Way Suite 300, University of Utah, Salt Lake City, Utah 84105, USA; JMOORE@EGI.UTAH.EDU
**Utah Geological Survey, Salt Lake City, Utah 84114, USA
***Mighty River Power Company, Hamilton, 3240 New Zealand
§Lawrence Livermore National Laboratory, Livermore, California 94550, USA
§§Pertamina - Geothermal Energy, Jakarta Pusat, 10340 Indonesia
§§§Department of Earth and Environmental Science, New Mexico Institute of Mining and Technology, Socorro, New Mexico 87801, USA

km and to depths below sea level. Deep wells drilled into the underlying liquid-dominated reservoir in the northern and central part of the volcanic ridge produce low salinity fluids representing recent recharge of meteoric and steam-heated water.

The evolution of volcanic-hosted vapor-dominated geothermal systems can be described by a five stage model. Stage 1 involves the formation of an over-pressured liquid-dominated geothermal system soon after magmatic intrusion. In Stages 2 and 3, pressures progressively decrease, and a curtain of steam-heated water surrounding a magmatic vapor-dominated chimney at 350°C and 14 ± 2 MPa develops. The relatively low pressure near the base of the chimney causes liquid inflow adjacent to the intrusion and the development of a secondary marginal vapor-dominated zone. In Stage 4, the magmatic vapor discharge from the intrusion becomes small, vapor pressure declines, and the secondary vapor-dominated zone expands above the intrusion. In Stage 5, the vapor-dominated zone floods because heat from the intrusion is insufficient to boil all liquid inflow. A more common, liquid-dominated volcanic-hosted system then develops.

INTRODUCTION

The majority of the world's geothermal systems are found on the flanks of andesitic volcanoes (Corbett and Leach, 1998). With relatively few exceptions, these systems are liquid-dominated, producing only low-salinity water at hydrostatic pressures. Detailed descriptions of liquid-dominated systems can be found in Ellis and Mahon (1977), Henley and Ellis (1983) and Corbett and Leach (1998).

Less common, and not as well understood, are the geothermal systems that discharge dry steam from vapor-dominated reservoirs. White and others (1971) concluded that vapor-dominated reservoirs form from liquid-dominated systems when discharge exceeds recharge. This imbalance occurs when marginal mineral seals restrict fluid inflow. Within vapor-dominated reservoirs, steam is the pressure controlling medium, although liquid water can be present as condensate within the fractures or remain within the pore spaces of the host rocks. Consequently, temperatures and pressures within vapor-dominated reservoirs generally remain relatively uniform with depth. While many vapor-dominated reservoirs have initial temperatures near 240°C and pressures of 3.1 to 3.4 MPa, higher temperatures and pressures can occur (White and others, 1971; Truesdell and White, 1973; Ingebritsen and Sorey, 1988). Because pressures are subhydrostatic, vapor-dominated reservoirs are underpressured with respect to the surrounding water saturated rocks and the pressure differences increase with depth. Volcano-hosted, vapor-dominated reservoirs have been found at Darajat, (Hadi and others, 2005), Kamojang (Suryadarma and others, 2005), Karaha-Telaga Bodas (Allis and others, 2000), Patuha (Layman and Soemarinda, 2003), Wayang Windu, (Bogie and Mackenzie, 1998; Asrizal and others, 2006) West Java, Indonesia, Puna, Hawaii (Richard, 1990), and Matsukawa, Japan (Hanano and Matsuo, 1990). Large vapor-dominated systems generated in response to the emplacement of shallow plutons occur at The Geysers, California and Larderello, Italy (White and others, 1971; Truesdell and White, 1973; Moore and Gunderson, 1995; Moore and others, 2000a). However, neither of these two large systems is volcano-hosted.

Few vapor-dominated geothermal systems have been recognized in the geologic record. Nevertheless, there is evidence that high sulfidation and some porphyry ore deposits may be intimately linked to the formation of vapor-dominated regimes. Fournier (1967, 1999) suggested that copper mineralization at Ely, Nevada, occurred when parts of the still crystallizing intrusion became vapor-dominated. High sulfidation ore deposits are characterized by advanced argillic alteration and leaching by acid SO_4 fluids within vapor-dominated chimneys that channel the upward migration of SO_2-bearing magmatic gases. The enhanced permeabilities of these acid altered zones subsequently control the distribution of later ore carrying fluids (Hayba and others,

1985; Stoffregen, 1987; Reyes and others, 1993; Hedenquist and others, 1994; Arribas, 1995).

Deep drilling at Karaha - Telaga Bodas on the flank of Galunggung Volcano, approximately 15 km east of Garut in West Java (fig. 1), has provided an unparalleled opportunity to characterize the hydrothermal evolution of a vapor-dominated, high sulfidation regime that formed within the last 6000 years (Allis and others, 2000; Moore and others, 2004a). In this paper, we first characterize the present temperature, pressure and hydrologic regimes within the geothermal reservoir. The evolution of the hydrothermal mineral assemblages preserved in the altered rocks and the fluid inclusions they contain are then described. Finally these observations are combined to develop a general model of the evolution of volcano-hosted vapor-dominated geothermal systems.

<center>ANALYTICAL METHODS</center>

<center>*Sample Selection*</center>

Hydrothermal alteration and rock distributions were studied in detail in four coreholes, T-2, T-8, K-21 and K-33 and in the deep production tests, TLG 1-1, TLG 1-1 ST2 (sidetrack), TLG 2-1, TLG 3-1, KRH 2-1 OH (original hole) and KRH 2-1 RD (redrill) to complement the existing well site logs. More than 3,900 m of continuous core and 14,800 m of cuttings were sampled as part of this investigation. The deep production wells were rotary drilled. Cuttings samples from these production wells were nominally thin sectioned and examined petrographically at 30 m intervals. Because of the significance of veins as fluid conduits and the inherent difficulties in deciphering vein assemblages in the cuttings samples, the core holes were sampled more frequently. Mineral identifications were routinely supported by X-ray diffraction analyses of bulk samples and clay (<5 micrometer) separates.

<center>*Fluid-Inclusion Measurements*</center>

Heating and freezing measurements were performed on fluid inclusions trapped in quartz, anhydrite, calcite and fluorite. The inclusions were studied in doubly polished plates of individual crystals hand-picked from the drill cores. Measurements were made on a Linkham THSMG 600 heating and freezing stage calibrated with synthetic fluid inclusions. The precision of the measurements is estimated to be $\pm$ 0.1°C at 0.0°C and $\pm$ 3°C at 374°C. Only measurements made on liquid-rich inclusions are reported. The salinities of two-phase inclusions with ice-melting temperatures >−21.2°C were calculated using the equation presented by Bodnar (1993). A few inclusions in quartz yielded ice-melting temperatures <−21.2°C. These inclusions displayed initial ice-melting temperatures near −50°C, suggesting the presence of Ca, Mg or Fe in addition to Na. Salinities of these inclusions were approximated from relationships in the system H_2O-NaCl-$CaCl_2$ (Oakes and others, 1990). The compositions of halite-bearing inclusions were calculated from halite-dissolution temperatures using the equation of Sterner and others (1988).

<center>*Scanning Electron Microscope Analyses*</center>

Scanning electron microscope (SEM) images and semi-quantitative analyses by energy dispersive spectroscopy (EDS) have provided critical information on textural relationships, mineral morphologies, and scale and mineral compositions. Small, freshly broken pieces of each sample were coated with C and examined on a Philips XL30 Environmental Scanning Electron Microscope (ESEM) at the Idaho National Engineering and Environmental Laboratory. This instrument is equipped with a Princeton Gamma Tech Prism system. An accelerating voltage of 20 kV and a beam diameter of 3 micrometers were utilized. A ZAF correction procedure was used to reduce the elemental compositions.
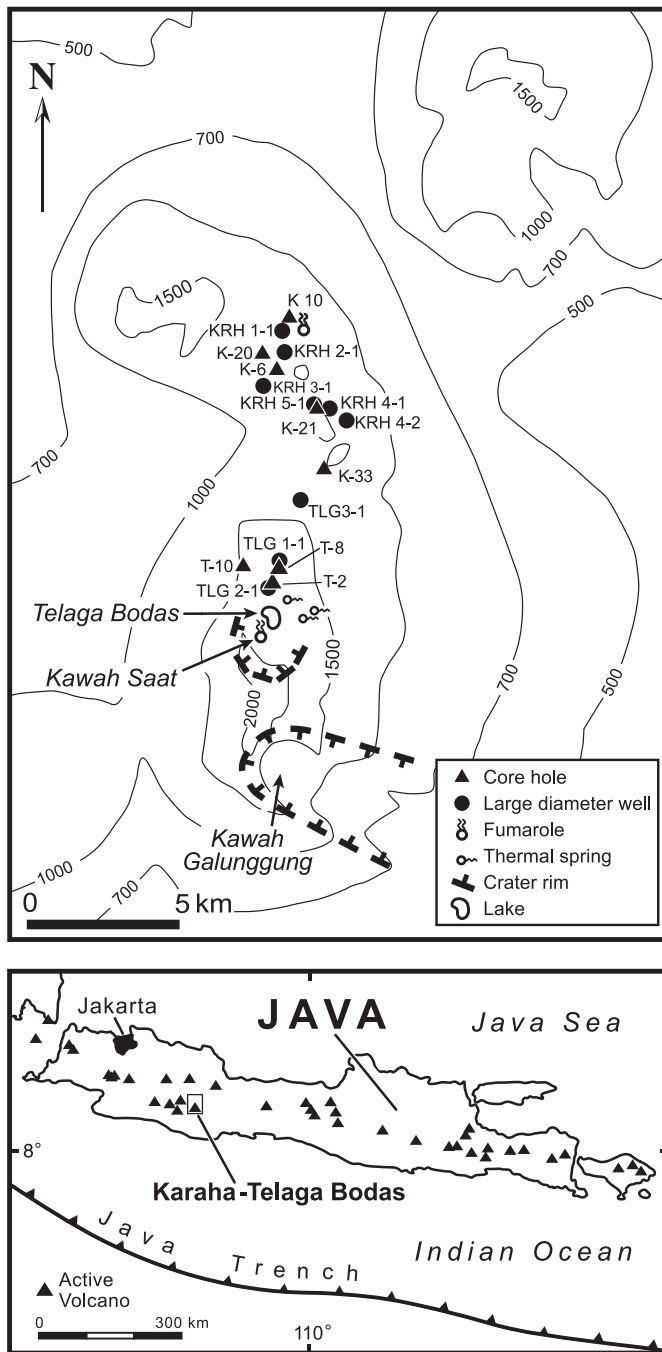
Fig. 1. Map illustrating the distribution of volcanic features, thermal manifestations and geothermal wells at Karaha – Telaga Bodas. Kawah Galunggung is the main vent of Galunggung Volcano. Telaga Bodas is an acid lake. Acid Cl-SO$_4$ springs discharge down slope of Telaga Bodas. Springs at Kawah Karaha discharge acid SO$_2$ or CO$_2$–rich waters. Only wells discussed in the text are shown. KRH and TLG series wells are deviated, rotary drilled large diameter wells. T and K series wells are vertical core holes. Contour lines show elevations in meters. Modified from Moore and others (2004a).

^{14}C Dating

Organic matter contained in core samples of three lake deposits was dated by accelerated mass spectrometry (AMS) at the Institute of Geological and Nuclear Sciences, Wellington, New Zealand. Material suitable for dating consisted of dispersed cellular organic matter with a few rare polypodiaceous fern spores that were oxidized and not identifiable as to species. No pollen was recognized. The bulk organic material, including charcoal, was used for radiocarbon dating. Each sample was crushed and treated with: 1) hot dilute HCl to remove carbonates; 2) room temperature HF to remove silica, silicates and metal oxides; 3) hot concentrated and dilute HCl to remove fluorides; 4) HNO_3 to convert decomposed organic material into alkali-soluble humic acids; and 5) KOH to eliminate contamination by younger humic acids. The remaining sample was sieved, combusted to CO_2, reduced to graphite, and dated. $\delta^{13}C$ values of -23.7 to -27.0 per mil were obtained directly on the CO_2. These values are typical of terrestrial organic matter.

Fluid Analyses

Fluid compositions were determined by standard chemical techniques. Concentrations of cations and SiO_2 were measured by atomic absorption spectrophotometry. The concentration of SO_4 was determined by ion chromatography. The samples were analyzed for Cl by titration and for B and NH_3 by colorimetric spectrophotometry. Sampling conditions and weirbox compositions of well waters are given in Appendices 1 and 2. Gas samples were collected in evacuated vessels containing NaOH and $CdCl_2$. CH_4, H_2, Ar and N_2 were analyzed by gas chromatography using a thermal conductivity detector, CO_2 by infrared analysis and H_2S by iodine titration. The O_2 content of the samples, determined by gas chromatography, was used to correct N_2 and Ar for air contamination. $^3He/^4He$ analyses were performed by R. Poreda at the University of Rochester, New York. The $\delta^{18}O$ and δD values of the fluids were determined at the Institute of Geological and Nuclear Sciences, Wellington, New Zealand.

THE KARAHA−TELAGA BODAS GEOTHERMAL SYSTEM

The Karaha - Telaga Bodas geothermal system is located beneath the volcanic ridge extending northward from Kawah Galunggung, the active vent on Galunggung Volcano (fig. 1). During the 1990s, the Karaha Bodas Co. LLC drilled 29 thermal gradient and deep production tests, some to depths close to 3 km, along a 10 km long section of the ridge between the thermal features at Telaga Bodas in the south and Kawah Karaha in the north (fig. 1, table 1). An extensive suite of downhole pressure and temperature measurements, fluid and rock samples, lithologic logs and geophysical data was collected. Temperatures exceeding 300°C were recorded in the deepest wells throughout the field. The highest measured temperature, 353°C, was encountered in the southernmost well, where the thermal anomaly is shallowest. Wells in the southern part of the field produce only dry steam from a vapor-dominated reservoir. Deep wells in the central and northern part of the field discharge low-salinity water from an underlying liquid-dominated zone.

Despite the extent of the geothermal system, and the high subsurface temperatures, surface manifestations are limited to the northern and southern ends of the prospect. These thermal features reflect the discharge of steam and the formation of acidic steam-heated water; no evidence for the discharge of deep NaCl water has been observed. Acid alteration, mud pots and fumaroles with temperatures up to 97°C occur at Kawah Saat, on the margins of Telaga Bodas, an acidic lake, and at Kawah Karaha. Telaga Bodas lies within a phreatic explosion crater surrounded by a rim of ejecta several meters high. An analysis of acid $SO_4−Cl$ water collected from the lake is shown in table 2. The low pH (0.4) and high concentrations of SO_4 (30500 mg/L) and Cl (8850 mg/L) reflect the influx of magmatic gases, including SO_2 and HCl (Heden-

Principal well facts

Well*	Total Depth (m)	True Vertical Depth (m)	Elevation Kelly Bushing (m)+	Elevation Total Depth (m)	Maximum T(°C)
K-6	614	614	1332	718	126
K-10	1311	1311	1193	-118	146
K-20	1018	1018	1289	271	180
K-21	1654	1654	1416	-238	259
K-33	2018	2018	1383	-635	256
KRH 1-1 ST2	3041	2829	1267	-1562	316
KRH 2-1 OH	3064	2842	1342	-1500	272
KRH 2-1 RD	2763	2649	1342	-1307	304
KRH 3-1 ST	3077	2970	1409	-1561	334
KRH 4-1	1849	1812	1387	-425	263
KRH 4-2 RD	2418	2316	1387	-930	249
KRH 5-1	2444	2436	1410	-1026	279
T-2	1383	1383	1670	288	321
T-8	1326	1326	1630	304	288
T-10	1586	1586	1460	-127	263
TLG 1-1 ST2	1782	1742	1629	-113	288
TLG 2-1	2588	2282	1677	-605	353
TLG 3-1	2480	2478	1435	-1043	296

*OH = original hole; RD = redrill; ST = side track. +Elevations are in meters with respect to sea level. The data were provided by Karaha Bodas Co. LLC.

quist, 1995) whereas the high cation contents are attributed to acid leaching and advanced argillic alteration of the surrounding volcanic rocks (Moore and others, 2004a). Acid Cl-SO$_4$ springs with temperatures up to 61°C discharge on the hill slopes east and north of the lake. Springs at Kawah Karaha discharge acid SO$_4$ or CO$_2$-rich steam-heated waters with a maximum temperature of 37°C. ^{3}He/^{4}He ratios of springs and fumaroles from the three thermal areas range from 7.1 to 7.7Ra (n = 6, unpublished data, Karaha Telaga Bodas Co. LLC). These isotopic compositions are typical of crustal fluids that extract heat from active, near-surface magmatic systems (Torgerson and others, 1982; Kennedy and van Soest, 2006).

Geologic Setting

Galunggung Volcano is one of several volcanic centers that form the volcanic ridge hosting the geothermal field. It is also among the most active of Indonesia's 128 volcanoes, having erupted 5 times since 1822, most recently in 1984 (Kimberly and others, 1998). The rocks of Galunggung Volcano include the Old Galunggung Formation, the Tasikmalaya Formation, and the Cibanjaran Formation. The Old Galunggung Formation is composed of ash-flow, air fall and lahar deposits and lava flows. Bronto (ms, 1989) estimated the age of this formation to be between 50,000 and 10,000 y BP, but these ages are not well constrained. The Tasikmalaya Formation consists of debris avalanche, lahar and pyroclastic deposits that accompanied collapse of the volcano's southeast flank and formation of Kawah Galunggung, the volcano's crater (Escher, 1925). The debris avalanche flow generated during flank collapse produced a hummocky deposit covering 170 km^2 and extending 23 km southeast of the crater (Bronto, ms, 1989) known as "The Ten Thousand Hills of Tasikmalaya"

TABLE 2

Compositions of representative reservoir and lake waters from Karaha-Telaga Bodas

Sample[*]	T (°C)[+]	Res Stm Frac (%)[¥]	pH[§]	Na	K	Ca	Mg	B	SiO$_2$	Cl	SO$_4$	HCO$_3$	nkc (°C)[#]	qtz (°C)[##]
K-33a	250	25	7.50	140	35.0	4.7	0.34	3.13	273	35.1	57.4	334	249	203
K-33b	250	25	7.30	133	33.8	3.9	0.75	2.97	331	37.8	84.4	304	251	219
KRH 2-1 RD	225	7	8.15	424	51.8	3.7	0.31	33.0	348	534	128	196	228	223
KRH 3-1 STb	265	15	8.33	497	95.5	2.6	0.02	43.4	541	826	58.5	64.8	268	267
KRH 4-1a	250	70	7.73	1313	201	24.8	0.04	106	391	2247	28.8	92.5	248	233
KRH 4-1b	250	74	7.80	1251	188	24.0	<0.01	103	365	2107	26.5	83.9	245	227
KRH 4-1c	250	67	7.73	1428	230	42.6	0.21	110	402	2450	21.9	72.8	247	236
KRH 5-1a	280	22	7.16	2983	832	675	0.92	102	110	6909	19.9	25.7	272	143
KRH 5-1b	280	34	7.01	2983	999	726	1.03	1.05	528	7014	13.8	30.8	285	264
KRH 5-1c	280	11	6.60	3547	1069	929	2.31	129	70	8033	3.6	<3.13	278	118
TLG 3-1a	220	85	7.28	770	112	46.7	0.01	165	502	1315	78.6	72.6	225	258
TLG 3-1b	220	88	7.11	671	101	77.5	0.02	189	148	1223	79.4	56.5	218	161
TLG 3-1c	220	88	7.01	769	120	143	0.03	144	186	1539	50.2	53.2	217	175
TLG 3-1d	220	87	7.00	794	132	190	0.02	303	424	1660	45.2	51.7	219	241
Telaga Bodas[^]			0.40	122	30.1	394	206	1.3	348	8850	30500			

Analytical values in mg/L. See Appendices 1 and 2 for sampling conditions, dates and weirbox compositions. [*]Multiple samples are labeled alphabetically. [+]Temperature of the principal reservoir feed zone. [¥]Calculated fraction of reservoir steam in the well discharge. [§]Laboratory pH. The pH of Telaga Bodas water was calculated from ion balance criteria (Moore and others, 2004a). [#]Temperatures calculated using the Na-K-Ca geothermometer (Fournier and Truesdell, 1973). [##]Temperatures calculated using the quartz geothermometer (Fournier and Potter, 1982). [^]Lake water. The sample contains 2320 mg/L Fe.

(Junghuhn, 1853). Charcoal from the uppermost of three pyroclastic flows overlying the debris avalanche deposit has yielded a ^{14}C age of 4200 ± 150 years BP (Bronto, ms, 1989). North of Kawah Galunggung, Telaga Bodas and Kawah Saat lie within a group of nested craters open to the north (fig. 1). The age of these craters has not been established. The Cibanjaran Formation, the youngest of the volcanic units, consists mainly of ash-flow, air fall and lahar deposits associated with eruptions occurring since 1822. Lava flows are a minor component of this formation.

Lava flows and volcanic bombs from Galunggung Volcano and dikes exposed in the crater walls range in composition from basalt to basaltic andesite (49 – 57 weight percent SiO_2; Bronto, ms, 1989). Older lava flows, pyroclastic deposits and intrusions of Miocene to Pleistocene age are dominantly andesite to dacite in composition (Budhitrisna, 1986). These rocks outcrop south of Galunggung Volcano and were found in the deep drill holes within the geothermal field.

The geothermal reservoir at Karaha – Telaga Bodas is developed primarily in pervasively altered pyroclastic deposits. Pumice fragments and glass shards are rarely observed, and where present, show little evidence of welding. Lava flows occur sporadically but most of the flow sequences are less than 100 m thick. The thickest accumulations occur in KRH 2-1 OH, which penetrated more than 575 m of dacite flows that may be part of a flow-dome complex.

Thin, discontinuous fine-grained tuffaceous sandstones and mudstones interpreted as lake beds are locally interlayered with the volcanic rocks. Their distributions suggest deposition in isolated basins. ^{14}C ages were obtained on organic matter from three of the lake beds; two from K-33 and one from T-8 (fig. 1). These samples yielded ages of 41,500 ± 1200 (K-33; -323 m elevation), 26,750 ± 170 (K-33; 49 m elevation) and 5,910 ± 76 years BP (T-8; 642 m elevation). The lake beds in T-8 are overlain by rocks that contain hydrothermal assemblages indicative of temperatures exceeding 300°C (see below). These age relationships indicate that T-8 was drilled at a site where nearly 1000 m of volcanic rocks accumulated during the last several thousand years.

Intrusive rocks were encountered below sea level in the three deep northern wells, KRH 1-1 ST2, KRH 2-1 OH, KRH 3-1 ST, and in the central part of the field in TLG 3-1. Samples from KRH 2-1 OH and TLG 3-1 were examined petrographically. KRH 2-1 OH encountered weakly altered medium grained granodiorite from −1359 m elevation to the base of the well. X-ray diffraction (n = 8) and thin section analyses indicate that it consists of approximately 20 weight percent quartz, 51 percent plagioclase, 13 percent potassium feldspar, and traces of magnetite and primary hornblende. Alteration minerals include a few percent each (2 – 8 percent) of actinolite, which replaces hornblende, epidote, illite and traces of tourmaline, which replace plagioclase, and chlorite, which replaces actinolite and plagioclase.

Dikes of granodiorite were encountered between −576 and −945 m elevation in KRH 2−1 OH and at depths below −764 m elevation in TLG 3−1. Those from KRH 2−1 OH have plagioclase-potassium feldspar-quartz ratios similar to the deeper, coarse grained granodiorite; samples from TLG 3−1 are relatively potassium-poor. Granodiorite was not encountered in the deep southern wells, TLG 1−1 ST2 and TLG 2−1, although its presence at shallow depths is implied by the occurrence of high temperature minerals similar to those found near the granodiorite in the north (see below). These mineral distributions indicate that the granodiorite extends from at least Kawah Karaha to Telaga Bodas. Furthermore, we suggest, based on the ^{14}C dating, that still cooling portions of the granodiorite provide the heat driving the geothermal system.

Fluid circulation is dominantly fracture controlled, although sedimentary rocks with high matrix permeabilities locally contribute to fluid production (Nemčok and others, 2004, 2006). Strike- and oblique-slip faults, normal faults, and tensile fractures occur within the low permeability rocks that cap the reservoir. The orientations of
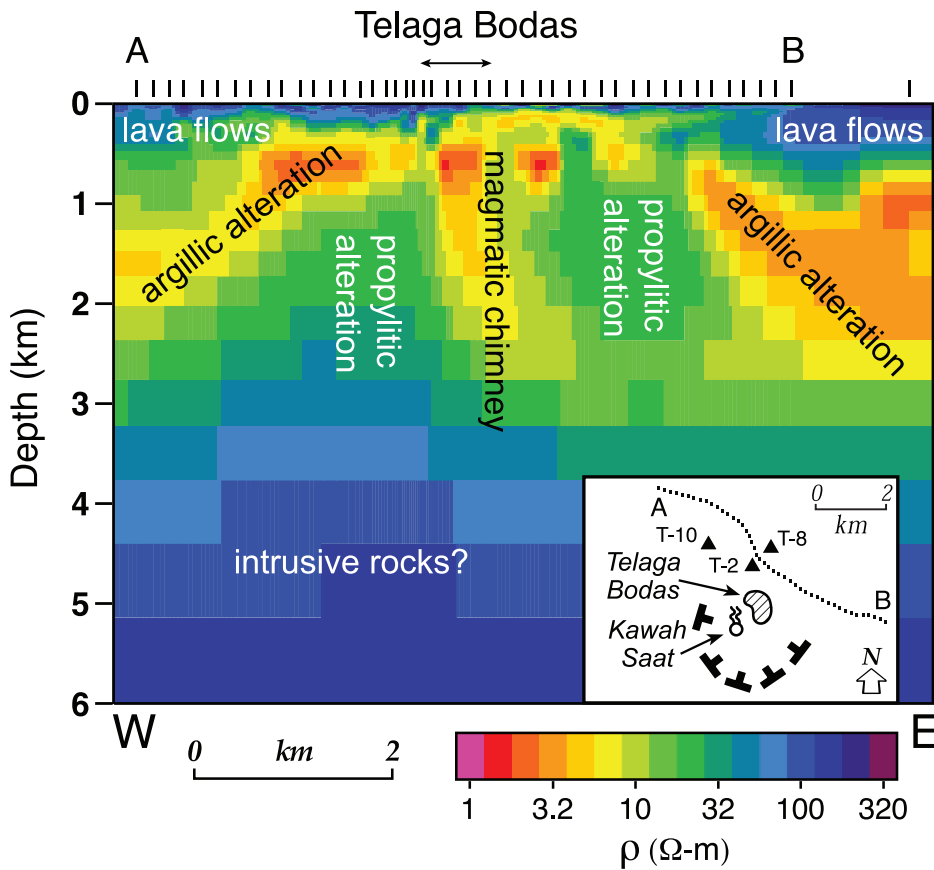
Fig. 2. Resistivity model resulting from joint TM mode/vertical magnetic field data along the profile labeled A-B in inset. The inversion image uses data from 47 closely spaced sites. Station locations are shown by tic marks at 0 depth. The geological interpretation of the major resistivity units is shown. The magmatic chimney is vapor-dominated. Surface elevations range from approximately 1000 m above sea level at the ends of the profile to 1700 m in the center near Telaga Bodas. No vertical exaggeration.

these fractures are controlled by the modern strike-slip stress regime. Normal faults and tensile fractures that formed within a normal-fault stress regime characterize the underlying reservoir. Productive fractures are approximately perpendicular to the minimum compressive stress ($\sigma_3 = 98°/0°$) and are prone to slip and dilation.

Geophysical Surveys

Gravity and magnetotelluric surveys were conducted to help characterize the geometry of the reservoir and the distribution of faults controlling fluid flow at depth. In 1996 and 1997, 47 closely spaced magnetotelluric (MT) soundings along an east-west profile were acquired by Karaha-Bodas Company LLC (fig. 2; Wannamaker and others, 2004). Because an increased fluid content due to fracturing and the formation of certain hydrothermal alteration minerals (for example, mixed-layer clays) can give rise to an electrical resistivity contrast, electromagnetic (EM) methods have been widely applied in geothermal exploration (Anderson and others, 2000; Cumming and others, 2000; Ussher and others, 2000). At the time of the surveys, artificial EM interference was inconsequential due to a lack of industrial infrastructure;

thus, the data quality is high. After minimal editing, a uniform electrical strike axis of N10°E was established, based on principal axes of the impedance, and used for all sites and frequencies in the survey area. This uniform electrical strike behavior, together with a generally north-south elongation of the topography and geothermal system, suggests that careful two-dimensional interpretation of the dense profile will yield useful results.

The profile data were inverted using a two-dimensional regularized inversion program based on Tarantola (1987) and DeLugao and Wannamaker (1996) to yield a detailed resistivity section of the upper 6 km (fig. 2). Inaccuracies from possible three-dimensional effects were reduced by emphasizing inversion of the TM mode plus the vertical magnetic field transfer functions (Wannamaker, 1999). The starting and *a-priori* model for the inversion was a smooth one-dimensional section obtained through integrating the TM mode impedance along the profile. Provided site sampling is good, this is equivalent to emplacing a single electrode line the entire length of the profile, which effectively cancels lateral heterogeneity effects within the profile and yields an average background (Wannamaker and others, 1997). The soundings each consisted of 25 frequencies of data running from ~100 to 0.003 Hz, and the inversion mesh contained 248 x 48 cells. The normalized root-mean-square (RMS) misfit from the inversion was 2.3, which is considered good for real-world field data.

In the model shown in figure 2, five distinctive resistivity regimes are recognized: (1) a thin resistive layer at the surface; (2) a conductive layer (<10 ohm-m) sloping to the northwest and southeast; (3) a moderately resistive (tens of ohm-m) region in the center in the 0.5 to 3 km depth range encapsulated by the conductive layers; (4) a vertical conductive structure inside the moderately resistive region; and (5) a resistive basement starting near 4 km depth. The thin surficial resistive layer can be correlated with thin lava flows displaying relatively little alteration. The sloping conductive layer is interpreted to represent the argillically altered rocks that form a cap rock over the geothermal system. Low-resistivity caps containing smectite and mixed-layer clays are a common feature of geothermal systems worldwide (for example, Ward and others, 1978; Pellerin and others, 1996; Cumming and others, 2000; Mustopa and others, 2003). The moderately resistive regime (3) beneath Telaga Bodas starting at depths of <1 km reflects a relatively shallow transition from more electrically conductive clay-bearing rocks to higher-grade and less conductive propylitically altered rocks. The formation of resistive bodies with high-temperature propylitic alteration is becoming a recognized feature in active andesitic systems (for example, Anderson and others, 2000; Ussher and others, 2000; Uchida and others, 2001, 2003; Uchida, 2003, 2005; Cumming and Mackie, 2006). At Telaga Bodas, the distribution of the deep alteration assemblages observed in wells to the north (T-2 and TLG 2-1), the presence of a magmatic component in the lake water, temperatures in excess of 350°C at shallow depths and the results of gravity surveys (see below) suggest that the central shallow block of moderate resistivity is underlain by intrusive rocks that are part of the granodiorite stock penetrated in the northern wells. Still higher resistivities characterize the deepest parts of the model, and here we may be encountering the intrusion itself.

Perhaps the most intriguing feature of the resistivity cross section is the central nearly subvertical conductive structure (<10 ohm-m) beneath Telaga Bodas. We suggest this structure represents the vapor-dominated chimney that provides a pathway to the surface for magmatic gases. The low resistivities at depth in the chimney could result from two different processes. First, high-salinity fluids can be directly exsolved from a magma (Shinohara, 1994). Alternatively, the formation of acid SO_4 water by disproportionation of magmatic SO_2 to H_2S and H_2SO_4 (Bethke, 1984), and its interaction with the chimney host rocks, can result in the formation of fluids with

salinities often exceeding several weight percent (Arribas, 1995). These are sufficient in small amounts to cause the low resistivity of the imaged chimney structure (Nesbitt, 1993). Even though acid cation-leached rocks and advanced argillic alteration were not encountered in the deeper portions of the southern wells, the composition and very low pH of the Telaga Bodas water sample (table 2) provides direct evidence for the influx of magmatic SO_2 to the lake from within the chimney below. The cross section and its interpretation closely resemble the model of the Alto Peak geothermal system in the Philippines developed by Reyes and others (1993). We believe this is the first direct geophysical image of such a magmatic vapor-dominated chimney and its properties.

The resistive region of propylitic alteration correlates with a +10 mgal gravity anomaly centered near Telaga Bodas (Tripp and others, 2002). Their two-dimensional density model portrayed an inverted triangular feature of uniform density contrast and a depth to its top of about 600 m. However, they note that the fit to the measurements by a sphere with a similar depth and density contrast is essentially as good, highlighting the non-uniqueness of potential field data. We also expect it is possible that a more vertical cylindrical structure of diminishing density contrast with depth could provide a reasonable fit. Although Tripp and others (2002) initially interpreted this object to be the intrusion itself, we prefer to assign the feature to densification caused by propylitic alteration consistent with the mineral relationships observed in the wells and its correspondence with the moderately resistive shallow block of figure 2.

Reservoir Temperature Distributions

Temperature and pressure measurements were obtained from most wells. With few exceptions, the surveys were conducted days to months after the wells were disturbed by flow or injection testing. The history of logging in each well has been carefully examined to identify the main feed-zones controlling the pressure regime, the fluid state at those feed-zones, and portions of the logs that appear to be recording true host-rock temperatures (for example, portions not affected by well-bore or casing annulus flow). In general, zones exhibiting isothermal profiles have been excluded from the temperature analysis, apart from the inflow points to the inferred internal flows. In some cases, static gas accumulations in the upper part of the well bore indicated the approximate host-rock temperature. Temperatures and pressures are shown in figures 3 and 4, respectively. Figure 5 shows a conceptual model of the system derived from these data. All of the data are based on inferred steady-state conditions; no corrections for apparent transient conditions have been applied. This is probably a major cause of the scatter in the composite pressure and temperature trends. Figure 3 shows that temperatures in many of the northern wells follow a linear, apparently conductive heat flow trend with a gradient of 115°C/km. This appears to represent a background thermal regime. At elevations above ~1100 m, temperatures are nearly isothermal owing to downward-percolating meteoric and steam-heated water in the vadose zone. Wells in the central and southern parts of the system can be differentiated by higher temperatures. The deepest wells, KRH 1-1 ST2 and KRH 3-1 ST, encountered temperatures of ~320°C at −1500 m elevation. KRH 3−1 ST, the hottest of the northern wells reached a temperature of 334ºC at total depth. Assuming that the temperature gradient can be extrapolated into ductile, impermeable rock at greater depth, the elevation where partial melt temperatures (~800°C; Fournier, 1999) in the upper crust will be reached is at ~5.7 km below sea level. This suggests that the entire geothermal system may be underlain by a substantial thermal anomaly characterized by partial melt conditions in the middle to upper crust.

Wells with an intermediate trend, largely in the central part of the geothermal system, (KRH 2-1 RD, KRH 4-1, KRH 5-1, TLG 3-1 ST, K-6 K-20 and K-33) record higher near-surface temperatures than wells further to the north. KRH 3-1 ST, in the west and
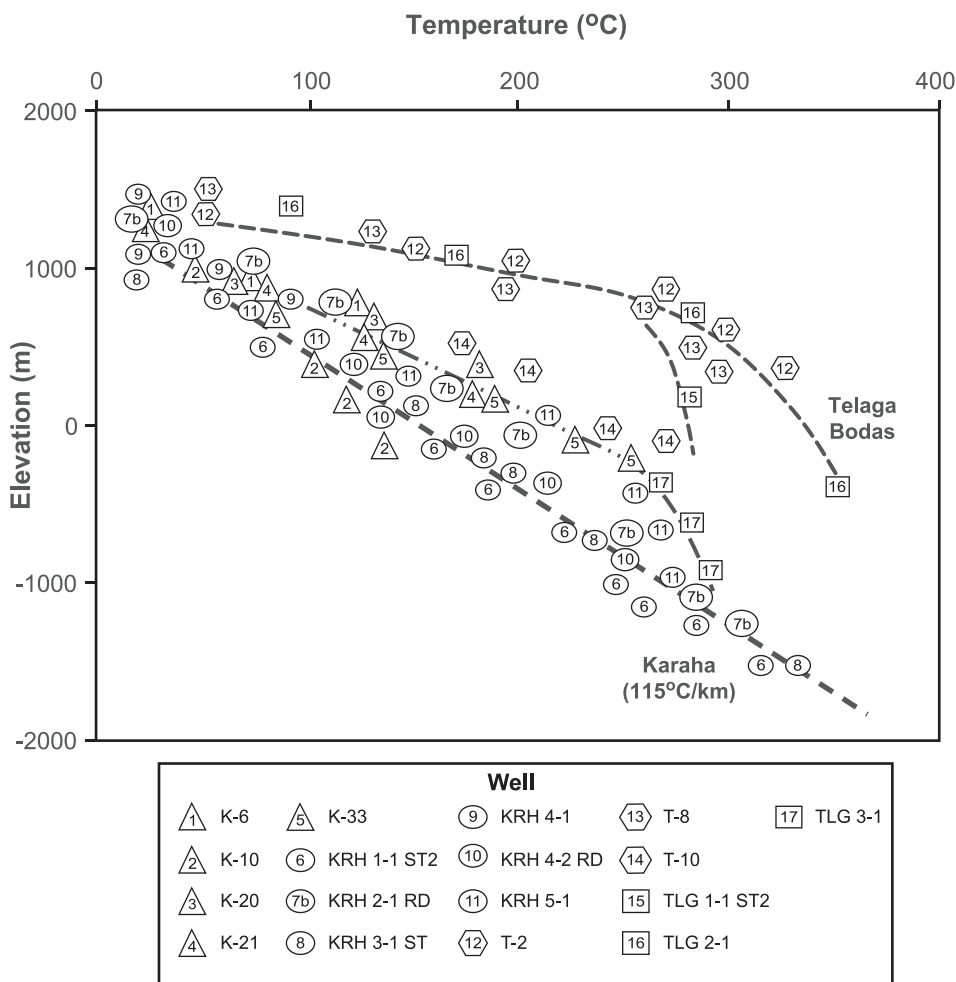
Fig. 3. Composite graph of the temperature data with respect to elevation. The data define three trends: a southern trend (Telaga Bodas), an intermediate trend (largely central parts of Karaha -Telaga Bodas system) and a northern trend (Karaha). See figure 1 for well locations.

KRH 4-2 RD in the east have lower temperatures, consistent with the background conductive heat flow trend to the north. The central area has a nearly constant temperature gradient of ~170°C/km down to about sea level, but is underlain by a zone with temperatures of 250° to 290°C between sea level and −1 km elevation. Steam entries occur in KRH 5-1, KRH 4-1, TLG 3-1 and K-33 in the depth range of 0 to −500 m elevation, with liquid entries typically found at greater depth. The area around KRH 2-1 RD, K-6 and K-20 includes a region of elevated temperatures at shallow depths, but at greater depth temperatures decrease to the background temperature gradient.

The central region with elevated temperatures below sea level and steam feed zones at >200°C is elongate, extending for at least 4 km in a north-south direction between wells KRH 5-1 and TLG 3-1 (fig. 1). Based on the background thermal regimes in wells KRH 3-1 ST and KRH 4-2 RD, the steam zone is less than 1 km in width in an east-west direction. This region appears to delineate a zone where vertical permeability between 0 and −1 km elevation has allowed a steam zone to form above a locally
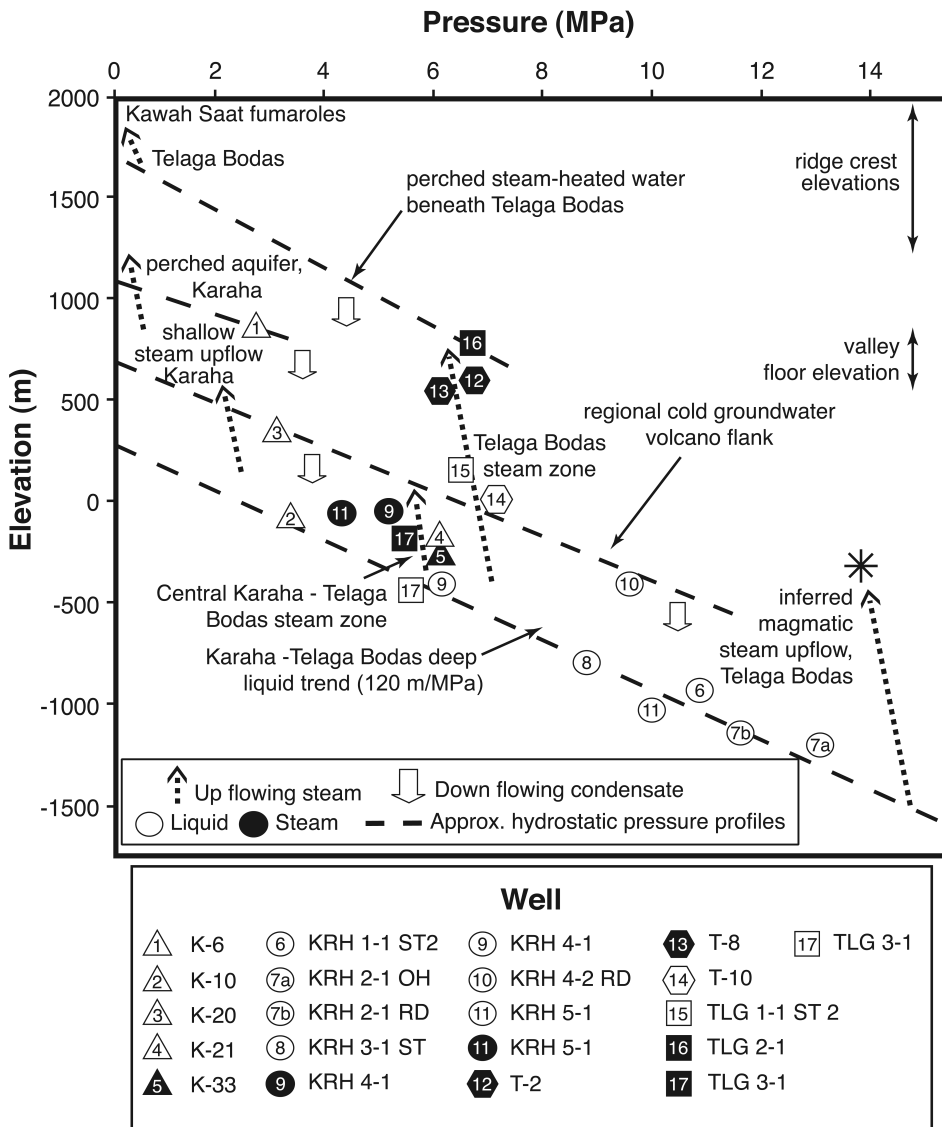
Fig. 4. Composite graph of pressure data with respect to elevation. Highlighted trends are discussed in the text. For reference, ridge crest and valley floor elevations are shown on the right hand side of the figure.

boiling liquid. Well T-10, 2 km northwest of Telaga Bodas, has a temperature profile similar to other wells in the central area. This well has a temperature of 266°C at its total depth (−127 m elevation). It is not known if a steam zone also underlies this well.

Temperatures in the Telaga Bodas area are significantly higher than those in the central part of the field. The abundant fumaroles around the lake and at Kawah Saat suggest considerable steam flow to the surface and locally boiling water at depth. The drill hole data indicate high temperatures, and a high temperature gradient exists down to at least 1 km elevation. In the vicinity of wells T-8 and TLG 1-1 ST2, a steam zone at 280° to 290°C is present to a depth of at least 200 m elevation. Further south, in
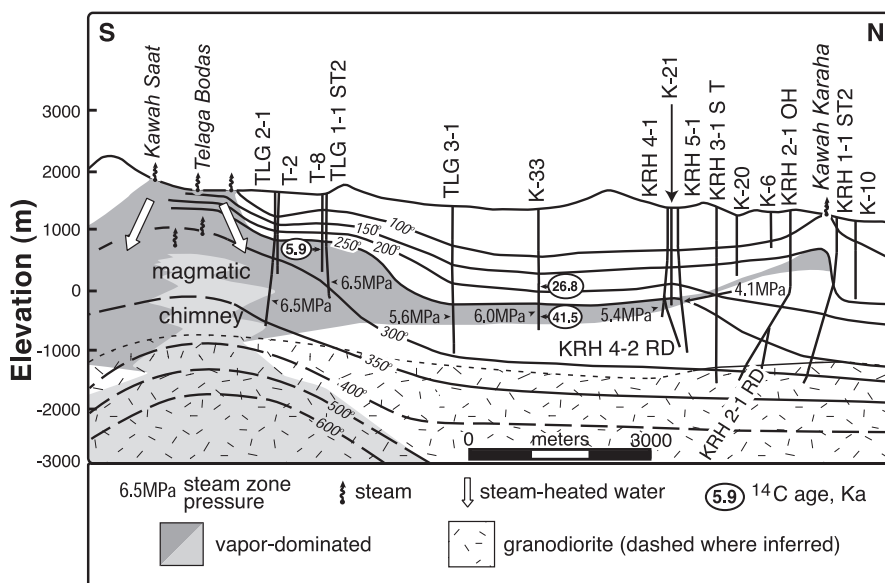
Fig. 5. Conceptual model of the geothermal system along the ridge axis showing temperature distributions as a function of elevation in m above sea level, the geometry of the steam and liquid zones based on flow tests and downhole measured pressures. Temperatures are shown as solid lines where measured and dashed where inferred. Regions in shades of gray are vapor-dominated. The magmatic vapor-dominated chimney is shown in light gray; surrounding portions of the vapor-dominated zone are dark gray. High-temperature hydrothermal minerals in TLG 1-1 ST2, TLG 2-1 and TLG 3-1, which indicate proximity to the intrusion, and the modeling of gravity data (Tripp and others, 2002) provide constraints on the depth and geometry of the granodiorite in the southern part of the field. Modified from Allis and others (2000).

the area of T-2 and TLG 2-1, higher temperatures occur between 700 and −200 m elevation, suggesting a gradient in temperature and pressure with increasing depth, implying liquid-dominated conditions. However, the discharging and static drill hole characteristics of these wells suggest that steam becomes the dominant flowing fluid at these depths once pressure drawdown occurs in the feed zones. The maximum measured temperature of 353°C occurs near the bottom of TLG 2-1.

Pressure Trends

For many drill holes, a single point representing the static pressure at the most prominent feed-zone has been selected from the logs. However, in some deep wells, a consistent pattern of isobaric steam over a liquid reservoir is apparent, allowing estimates of both steam zone and liquid zone pressures from the same log. When the pressure measurements are compiled onto one graph (fig. 4), a single, liquid-reservoir pressure trend can be defined beneath the Kawah Karaha and central regions of the field. The slope of the trend, 120 m/MPa, is that expected from water at >200°C. This indicates that between ~0 and −1000 m elevation (the ridge is at ~1500 − 2000 m elevation), there is sufficient horizontal permeability to prevent compartmentalization of the reservoir.

The hydraulic head in the liquid-dominated reservoir under the crest of the ridge is at an elevation of ~300 m. In contrast, the hydraulic head on the ridge flanks is at ~650 m elevation (fig. 4). Thus, the reservoir is underpressured by ~350 m (that is, 3.5 MPa) relative to the flanks. Because of this head difference, there is the potential for water to flow from the ridge flanks into the reservoir. If the groundwater level in the

adjacent valleys is near the ground surface, there is also the possibility that the system is being recharged from beneath the adjacent valley floors.

Pressures that plot at a significantly higher elevation than the deep hot liquid trend must represent either steam zones or perched aquifers. In the case of the central steam zone at about sea level, the pressure increases laterally from 4 MPa in the north in KRH 5-1 to close to 6 MPa in the south. Pressures of 6 to 6.5 MPa have been found at shallower depths of 0 to 800 m elevation in the Telaga Bodas steam zone. The pressure at greater depth beneath the Telaga Bodas area is uncertain, but using the 353°C temperature measured in TLG 2-1 as a guide, if this is in two phase equilibrium with saline fluids, then the pressure is in the range of 12 to 16.5 MPa for salinities of 30 percent to 0 percent respectively (fig. 4; see Fournier, 1987).

Perched water beneath Telaga Bodas could extend from the surface of the lake at 1710 m elevation to depths below sea level, given the inferred 14 MPa pressure beneath the TLG 2-1 and T-2 area (fig. 4). However, further north around TLG 1-1 ST2 and T-8, steam pressures of 6 to 6.5 MPa occur below ~1000 m elevation. Normally a stable liquid-over-steam interface is characterized by steam pressures slightly in excess of the liquid pressure, with low permeabilities around the interface preventing large-scale down flow of liquid (Ingebritsen and Sorey, 1988). Examination of core samples and thin sections show that low fracture permeabilities result from the deposition of anhydrite and calcite.

Steam-heated features at the surface in the vicinity of Telaga Bodas and Kawah Saat suggest that temperatures in the underlying rocks are at the boiling point. Further north near T-2 and T-8, however, a linear temperature profile from the ground surface to 1000 m elevation suggests relatively impermeable rock and sub-boiling conditions. T-10, 2 km west of T-8, also has an apparently conductive gradient to its total depth at −127 m elevation with a temperature of 263°C, and a liquid pressure profile indicating a relatively high head of ~800 m elevation. This well may be in a relatively impermeable thermal boundary zone to the west of the under-pressured region beneath the volcanic ridge.

Drill holes closest to Kawah Karaha indicate the presence of perched water tables, especially in the area of K-6 and K-20. The conductive temperature gradient at depth beneath this area suggests local boiling conditions in the perched aquifers, overlying a single-phase liquid.

Reservoir Liquid Compositions

Weirbox samples were collected during rig tests while drilling and later during well flow tests (Appendix 1). The compositions of the reservoir liquids, corrected to the downhole conditions, were calculated following the method of Truesdell and Singers (1974) and are given in table 2.

The most striking feature of the reservoir compositions are their diversity. This diversity is related to several processes. Samples KRH 2-1 RD, KRH 3-1 STb and K-33a and K-33b are comparatively dilute. These wells flowed at low rates and samples were collected after flowing for only 1 to 2 days. Thus their compositions likely reflect dilution by meteoric drilling water. However, low Mg concentrations and Na-K-Ca and quartz geothermometer temperatures (Fournier and Truesdell, 1973; Fournier and Potter, 1982) close to measured temperatures suggest that these waters have equilibrated, at least partially, with the reservoir host rocks at high temperatures.

Samples from wells KRH 4-1, KRH 5-1 and TLG 3-1 have compositions that stabilized during the flow tests and therefore are not considered to be contaminated. These wells have reservoir Cl concentrations ranging from 1539 to 8033 mg/L. Na-K-Ca geothermometer temperatures are close to the measured temperatures, but temperatures based upon quartz solubility are variable and generally lower.
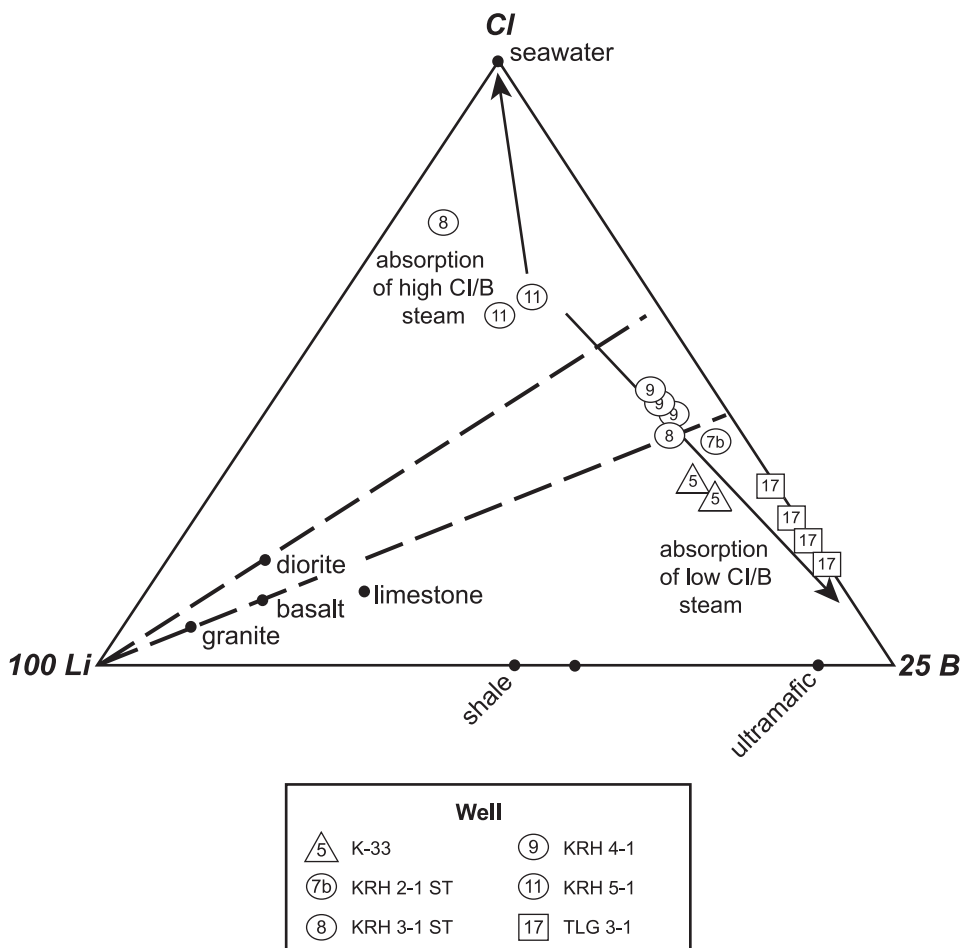
Fig. 6. Relative concentrations of Li, Cl and B in samples from Karaha - Telaga Bodas and representative rocks on a weight basis (after Giggenbach, 1991). See Appendix 2 for weirbox analyses. The trend lines suggest absorption of steam with varying C/B ratios.

Large variations in the Cl/B ratios of the fluids suggest that compositional differences are, in part, due to the addition of steam with variable Cl/B ratios. Figure 6 illustrates the relative concentrations of Li, Cl and B (Giggenbach, 1991) of representative reservoir waters. These samples define a trend originating near the Cl/B ratio of diorite and KRH 5-1, and extending toward lower Cl/B ratio values. Giggenbach (1991) suggests this trend reflects the addition of progressively lower Cl/B steam.

Reservoir Gas Compositions

Separated steam samples were collected during most of the well tests. All of the flow tests yielded enthalpies above those for a single phase liquid at the temperature indicated by the liquid geothermometers. This implies a contribution from either a resident reservoir vapor, (for example, a steam zone) or steam from *in-situ* boiling of reservoir liquid during the flow test. The gas compositions of the samples are shown in table 3.

Gas geothermometers based on H_2S, H_2S - H_2, CO_2 - CH_4 - H_2 (Fischer-Tropsch equation) and $N_2 – NH_3 – H_2$ yield unreasonably high or inconsistent temperatures, as

TABLE 3

Gas compositions of geothermal fluids

Sample[*]	Date	Stm Press (MPa g)[§]	Stm Fract (%)[¥]	Air (%)	Total Gas (wt%)	Mole percent of dry gas						
						CO_2	H_2S	NH_3	Ar	N_2	CH_4	H_2
K-33a	12/1/97	0.44	40	4.57	20.0	95.8	2.64	0.190	0.0075	0.481	0.556	0.326
K-33b	12/1/97	0.44	40	0.56	28.7	96.1	3.11	0.051	0.0020	0.183	0.355	0.173
KRH 4-1a	9/13/97	1.36	72	2.05	4.5	93.8	3.60	0.607	0.0008	0.495	0.831	0.692
KRH 4-1b	9/13/97	1.36	72	0.02	4.5	93.1	4.02	0.897	0.0042	0.430	0.812	0.706
KRH 5-1a[+]	12/17/97	0.55	34	0.03	1.1	92.4	4.41	0.799	0.0149	1.043	0.641	0.578
T-2	10/18/97	1.31	92	0.18	7.8	97.0	1.87	0.161	0.0022	0.247	0.321	0.403
T-8,a	7/13/97	0.22	97	0.57	8.3	90.4	8.07	<0.027	0.0002	0.119	0.009	1.35
T-8,b[++]	7/26/97	0.54	95	0.00	8.2	91.8	10.0	0.019	0.0005	0.200	<0.007	2.63
TLG 1-1[+]	12/1/97	1.31	94	0.06	3.6	80.8	10.4	0.017	0.0724	6.64	0.100	1.80
TLG 2-1a	2/18/98	0.93	95	0.21	21.5	96.9	1.07	0.220	0.0017	0.193	0.400	1.17
TLG 2-1b	2/18/98	0.93	95	1.69	29.6	97.8	0.51	0.412		0.919	<0.002	0.008
TLG 3-1a[+]	2/23/98	0.16	93	0.17	0.5	84.8	10.5	1.644	0.0255	2.27	0.060	0.745

[*]Multiple samples are labeled alphabetically. [+]Aerated drilling fluid contamination. [++]Gases sum to 104.7%. [§]Steam pressure (MPa gauge). [¥]Steam fraction.
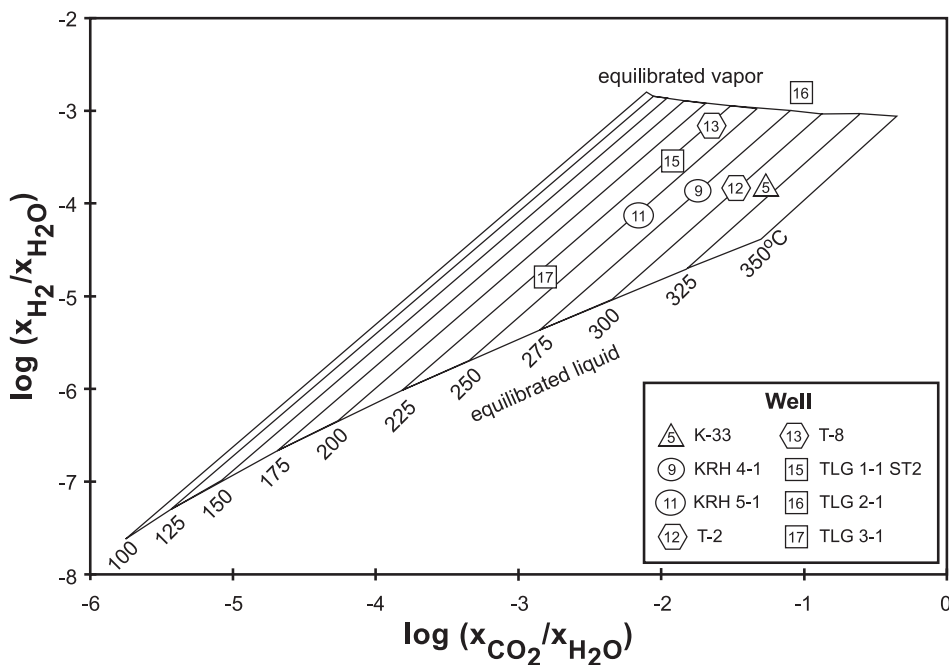
Fig. 7. Evaluation of H_2-H_2O, CO_2-H_2O equilibration conditions. Modified from Giggenbach, 1991 (see text).

is frequently found in geothermal systems (see Arnórsson and Gunnlaugsson, 1985; Giggenbach, 1991) and indicate enrichment in H_2S above the equilibrium values. However, the samples do display a consistent grouping on a CO_2-H_2 geothermometer grid (fig. 7). This grid is based on the CO_2/Ar - H_2/Ar ratio grid proposed by Giggenbach (1991). Application of the geothermometer grid assumes that CO_2 is fixed by equilibria between calcite and Ca-Al- silicates (Giggenbach, 1984, 1988). H_2 provides a measure of the redox conditions. The fugacity of H_2 is related to the variable R_H (Giggenbach, 1987) by the expression:

$$R_H = \log(f_{H2}/f_{H2O}) \tag{1}$$

At equilibrium between aqueous fluids and rock with approximately equal amounts of Fe^{+2} and Fe^{+3}, R_H is essentially constant at a value of -2.8, at temperatures of geothermal interest (Giggenbach, 1987).

In the original formulation of the grid, the concentration of Ar is used to estimate P_{H_2O}. In this case, it is assumed that the Ar concentration in the reservoir water is the same as in air-saturated groundwater, which is usually the largest component of hydrothermal waters (Giggenbach and Goguel, 1989). The modified grid shown in figure 7 utilizes the measured gas/steam ratios and includes a correction for the compressibility of steam. The liquid equilibration line represents equilibration of gas in an entirely aqueous environment whereas the equilibrated vapor line represents gas equilibration in the vapor phase. Samples plotting above the liquid equilibration line represent equilibration under two-phase conditions, or possibly an R_H greater than -2.8. Samples plotting below the line indicate H_2 re-equilibration at lower temperatures or an R_H less than -2.8 (Powell, 2000). The consistency between measured and
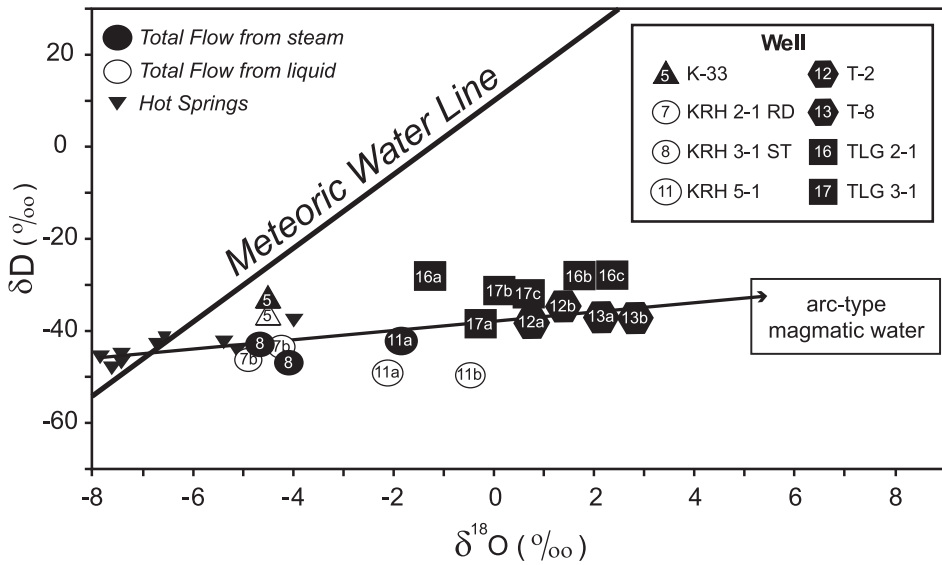
Fig. 8. Stable isotope compositions of Karaha - Telaga Bodas spring and well samples. The samples define a trend toward the composition of magmatic water defined by Giggenbach (1992). The meteoric water line is taken from Craig (1963).

predicted temperatures suggests that the gases equilibrated in a two phase environment.

Geothermometer temperatures range between 225°C and 310°C, and are similar to the measured temperatures in the wells. The apparent success of this geothermometer in predicting the reservoir temperature is consistent with the widespread occurrence of calcite in the rocks. This suggests that CO_2 and H_2 approach chemical equilibrium in the reservoir, whereas the other gases do not. Furthermore, the CO_2 and H_2 relationships indicate that the oxidation state in the reservoir is close to an R_H of -2.8, and that the system is mature and rock-dominated, as defined by Giggenbach (1993). Hydrogen gas concentrations indicative of a less mature, fluid-dominated, and more purely "magmatic" system would be expected to fall below the grid in figure 7, reflecting a more oxidized redox state. The apparent lack of equilibration among the other gases suggests that they may, instead, be controlled by local sources, or that the residence time is too short to reach equilibrium. A potential source of CH_4 and NH_3 is the breakdown of organic matter in the reservoir rocks whereas H_2S may be magmatic in origin.

Stable Isotopes

Samples of steam and liquid collected during the well tests were analyzed to determine their $\delta^{18}O$ and δD values. To assess data quality, steam and liquid analyses were separately corrected to the total discharge composition, assuming the steam fraction of the flow test and isotopic equilibrium at separation conditions. Because isotopic equilibration at separation is rapid, this approach provides a way to assess the uncertainty in the combined analyses and flow test data. Corrections to liquid analyses from well tests with a steam fraction of >90 percent produced erratic results and are not included. The results of the analyses are plotted in figure 8. The similarity of the total discharge compositions from liquid and steam samples demonstrate that uncertainties in the analyses and flow test data are relatively small. Most of the hot spring

samples cluster on the meteoric water line between δD values of −40 to −50 per mil. Some successive flow test samples (labeled a, b, c) show a progressive migration away from meteoric water toward greater $\delta^{18}O$ values, indicating decreasing contamination by drilling water.

The stable isotope compositions of the well samples suggest that they either contain a significant component of magmatic water, as defined by Giggenbach (1992), or they have equilibrated with un-exchanged intrusive rocks.

<div align="center">HYDROTHERMAL ALTERATION OF THE RESERVOIR ROCKS</div>

Four distinct mineral assemblages define the evolution of the geothermal system (Moore and others, 2004a). The earliest assemblage records development of a high-temperature liquid-dominated system. It is characterized by illite, epidote, actinolite, biotite and tourmaline. The second is represented by an episode of amorphous silica, chalcedony and quartz deposited as the early reservoir liquids boiled off. This mineral assemblage is distinctive and provides a unique time line that can be traced across the entire field. The third assemblage, characterized by calcite, anhydrite and wairakite, records the influx of steam-heated water. The final assemblage represents the complete boiling off of the geothermal fluids. This assemblage is characterized by the precipitation of NaCl, KCl and $FeCl_x$ on rock surfaces.

<div align="center">*Assemblage 1*</div>

The earliest hydrothermal assemblage can be broadly divided into an upper zone of argillic alteration characterized by clay minerals, carbonates and zeolites, an intermediate zone of propylitic alteration dominated by epidote, chlorite and actinolite and a deep, high temperature biotite zone characterized by biotite and tourmaline. The field-wide distributions of the key minerals defining assemblage 1 are shown in figure 9.

Throughout the field, the pyroclastic deposits are more extensively altered than the lava flows, and this feature persists through all stages of alteration. At shallow depths, pervasive argillic alteration of the groundmass of both the pyroclastic deposits and lava flows is dominated by smectite and mixed layer illite-smectite and chlorite-smectite. Quartz and pyrite are intergrown with the clay minerals in the pyroclastic deposits. Both plagioclase and ferromagnesium minerals are altered to clay minerals and carbonates, although alteration of phenocrysts in the lava flows is frequently weak. In other geothermal systems, smectite is typically not stable at temperatures above 180ºC, whereas the transition from mixed – layer clays to chlorite and illite is commonly essentially complete by ~225ºC (Henley and Ellis, 1983; Reyes, 1990).

Veins and vugs in argillically altered rocks at Karaha – Telaga Bodas are filled primarily with calcite, accompanied in places by zeolites (often laumontite), pyrite, and mixed layer chlorite-smectite. Carbonate veins are commonly deposited by CO_2–rich steam-heated water that forms an umbrella like halo around the high-temperature upflowing chloride water (Mahon and others, 1980; Hedenquist, 1990). The steam-heated water can descend along marginal fractures, cooling the reservoir and diluting the higher temperature water at depth.

The appearance of epidote (fig. 9) defines the top of the propylitic zone and the approximate base of the cap rock, which is characterized by steep temperature gradients indicative of a conductive regime. Epidote, illite, chlorite, pyrite, albite, quartz, and adularia occur in the upper part of the propylitic zone (figs. 10A and 10B). These minerals pervasively replace the groundmass of the pyroclastic deposits and lava flows. Plagioclase phenocrysts are altered to epidote, illite, calcite, albite, adularia and chlorite whereas the ferromagnesium minerals are replaced by chlorite, epidote, calcite, pyrite and Fe and Ti oxides. Only chlorite, epidote and pyrite, either intergrown or deposited separately, are common as vein minerals. In T-2, chlorapatite was
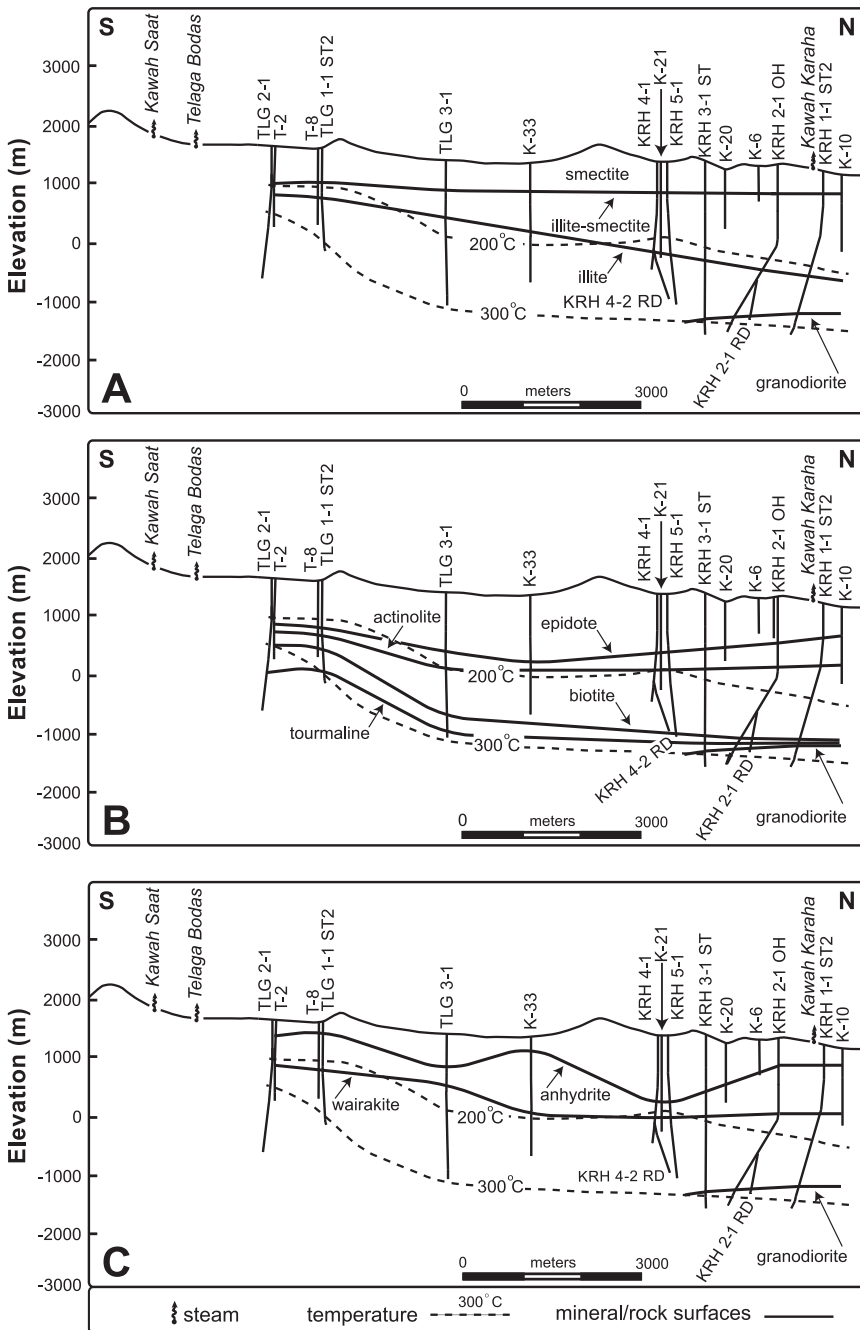
Fig. 9. North-south sections showing surfaces representing the first appearances of key minerals, the present-day 200° and 300°C isotherms and the top of the granodiorite. Elevations are in meters. A and B are representative of assemblage 1; C of assemblage 3. (A) The first appearance of mixed layer illite - smectite and illite. Smectite is present above the illite-smectite zone. (B) The first appearances of epidote, actinolite, biotite and tourmaline. The epidote surface defines the top of the propylitic zone; the appearance of biotite marks the top of the biotite zone. (C) The first appearances of anhydrite and wairakite.
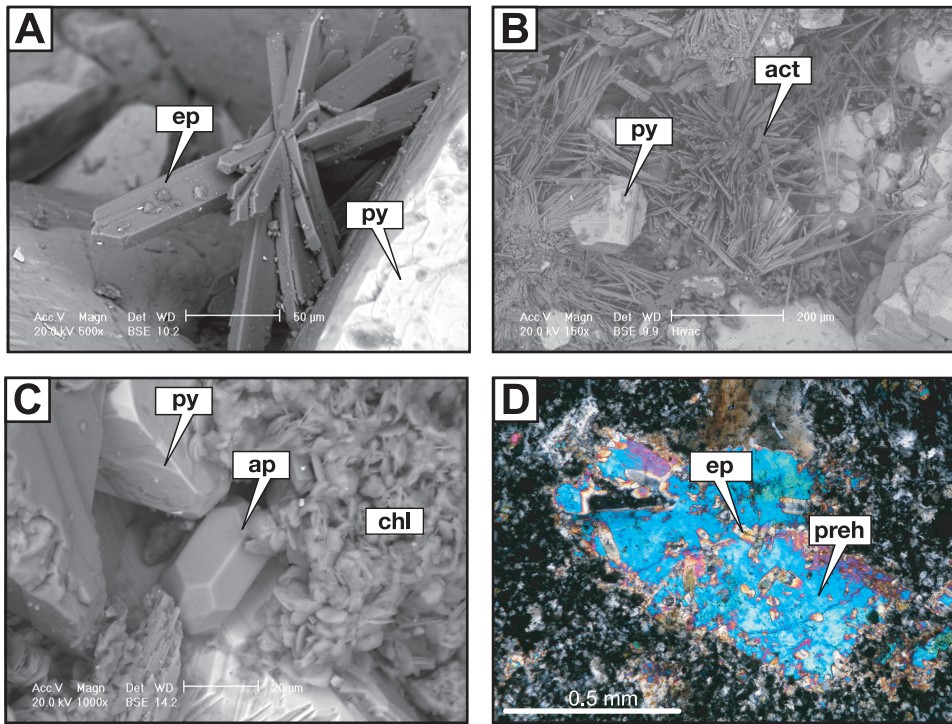
Fig. 10. Minerals and textures typical of propylitically altered rocks (assemblage 1). (A) SEM back-scattered electron image of epidote and pyrite. From 691 m elevation in T-2. (B) SEM back-scattered electron image of intergrown actinolite and pyrite. From 586 m elevation in T-8. (C) SEM back-scattered electron image of apatite, pyrite and chlorite. From 783 m elevation in T-2. (D) Photomicrograph of prehnite encapsulating numerous small crystals of epidote. From -369 m elevation in K-33. Crossed nicols. Abbreviations: act = actinolite; ap = apatite; cal = calcite; chl = chlorite; ep = epidote; preh = prehnite; py = pyrite.

deposited with chlorite and pyrite but, this mineral has not been found in other wells (fig. 10C). Epidote is widely distributed in geothermal systems appearing at temperatures of 240° to 260°C (Browne, 1978; Reyes, 1990). Sparse measurements on fluid inclusions trapped in coarse-grained epidote from the propylitic zones of other geothermal systems has yielded temperatures ranging from ~290° to 335°C (Moore and others, 2004b).

Actinolite first appears at slightly greater depths than epidote. It replaces ferromagnesium minerals and occurs with epidote and rare crystals of garnet in veins and vugs. The garnet that forms at this grade of alteration may be hydrated (Leach and others, 1983). Actinolite first appears in geothermal systems at temperatures of 280° to 300°C (Browne, 1978).

Prehnite was the last calc-silicate mineral deposited in the propylitic zone in assemblage 1. It is found in veins in the central and northern parts of the field where it encapsulates crystals of epidote (fig. 10D). Prehnite is essentially absent in the southern wells. The formation of prehnite after epidote suggests that temperatures had peaked and were locally beginning to wane (see discussion below).

Rocks in the biotite zone have been altered to biotite, magnetite, epidote, actinolite and sporadic diopside, garnet, tourmaline, pyrite and cubanite. Biotite occurs in thin veinlets and as fine-grained crystals that replace plagioclase. Its shallow-

est occurrence is in the southern part of the field (fig. 9). Biotite first appears at temperatures of 300º to 325ºC in other systems (Elders and others, 1979).

Diopside occurs sporadically within the biotite zone. The most common occurrence of diopside is with biotite as a replacement of the groundmass of the rocks. Near the granodiorite contact, diopside is intergrown with garnet in recrystallized rocks. Diopside is indicative of temperatures >300ºC, whereas garnet occurring within the inner portions of the biotite zone typically forms at temperatures of 325º to 350ºC (Elders and others, 1979).

Within the biotite zone, tourmaline forms brown to blue-green crystals that replace plagioclase in the country rocks and granodiorite. It first appears at a distance of ~300 m from the intrusive contact. In the larger vapor-dominated systems at Larderello, Italy and The Geysers, California, tourmaline was deposited in the country rocks at distances up to ~600 m from the granitic intrusions during the early liquid-dominated stages of hydrothermal activity (Cavarretta and Puxeddu, 1990; Moore and Gunderson, 1995). Fluid inclusions in quartz intergrown with tourmaline at The Geysers record temperatures exceeding 400ºC. The limited extent of tourmaline in the biotite-zone at Karaha – Telaga Bodas, compared to Larderello and The Geysers is presumably due to the smaller size of its heat source.

As the geothermal system at Karaha – Telaga Bodas evolved, the tourmaline-bearing rocks were cross cut by lower temperature minerals. In the deepest parts of KRH 2-1 OH, tourmaline-bearing rocks are cut by veins of epidote intergrown with actinolite. The epidote is in turn encapsulated in still younger wairakite. These veins document waning temperatures near the granodiorite contact.

Assemblage 2

Assemblage 1 was followed by the deposition of amorphous silica, chalcedony, quartz and rare bladed calcite. Chalcedony is a fibrous microcrystalline mixture of quartz and mogenite, a monoclinic SiO_2 polymorph (Flörke and others, 1991; Heaney and Post, 1992; Gíslason and others, 1997). Typically, chalcedony has a botyroidal habit.

The distribution of the silica phases changes progressively with depth and temperature, as implied by the distribution of alteration minerals. At the shallowest depths and lowest temperatures within the argillic zone, sporadic occurrences of alternating bands of amorphous silica and chalcedony are found (fig. 11A). Near the top of the propylitic zone, chalcedony replaces earlier vein calcite or fills calcite lined vugs (fig. 11B). Within the propylitic zone, veins containing euhedral crystals of quartz cut epidote- and actinolite-bearing rocks. Rarely, the veins consist entirely of chalcedony (fig. 11C). Botryoidal textures found at the base of the quartz crystals (fig. 11D) suggest that silica deposition began with the precipitation of chalcedony. No evidence of a hiatus, such as corrosion of the chalcedony or hydrothermal minerals at the interface between the chalcedony and quartz has been observed, indicating that precipitation of the two silica polymorphs represents a single continuous event.

Quartz crystals of assemblage 2 are distinctive and can frequently be recognized by their curved "c" axes (figs. 11E and 11F), twinning that results in unusual growth forms (fig. 11F), the presence of botryoidal textures (refer to fig. 11D), and complex extinction patterns under crossed nicols (refer to fig. 12D). These unique quartz crystals and textures occur in every core hole examined. Thus they occur over a strike length of at least 7 km and to depths of 2 km. Only cuttings are available from greater depths. Because of the extensive amount of grinding the cuttings have undergone, these textures are difficult to identify in the deep rotary drilled wells. Consequently, the full distribution of assemblage 2 quartz has not been established.

The transition from assemblage 1 to 2 is represented by intergrowths of quartz and epidote, prehnite or sericite (fig. 13). In each case, the mineral intergrown with quartz
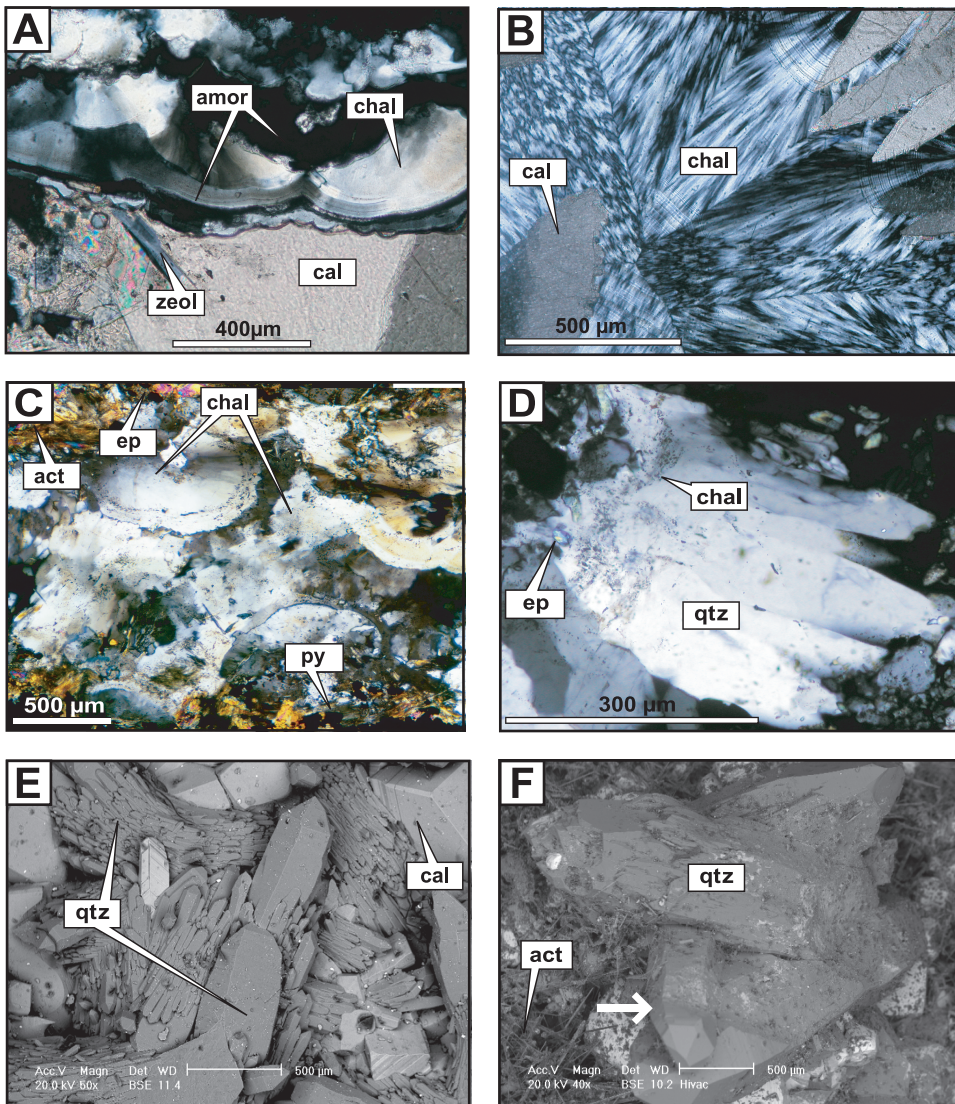
Fig. 11. Textures of silica minerals representative of assemblage 2. Photomicrographs shown in A-D were taken under crossed nicols. (A) Alternating layers of amorphous silica (black) and chalcedony (light gray). Calcite and a zeolite mineral were deposited after the silica polymorphs. From 626 m elevation in K-21. (B) Chalcedony filling a vug lined with calcite. From 829 m elevation in T-8. (C) Chalcedony vein cutting wall rocks containing epidote + actinolite + pyrite. From 492 m elevation in T-8. (D) Quartz overgrowths on chalcedony. Botryoidal textures are preserved at the base of the crystals. A grain of epidote is encapsulated in the chalcedony. From 428 m elevation in T-8. (E) SEM back-scattered electron image of quartz from 878 m elevation in T-2. A few younger blocky calcite crystals fill spaces between the quartz crystals. (F) Quartz crystals from 462 m elevation in T-8. The arrow points to a quartz crystal with a curved "c" axis. The quartz crystals postdate the actinolite needles in the lower left of the image. Abbreviations: amor = amorphous; act = actinolite; cal = calcite; cha = chalcedony; ep = epidote; qtz = quartz; py = pyrite; zeol = zeolite.

represents the youngest phase precipitated prior to quartz deposition. Figure 13A illustrates the textural relationships between epidote and quartz. Two generations of epidote are present; an early generation of prismatic epidote deposited in the wall rock
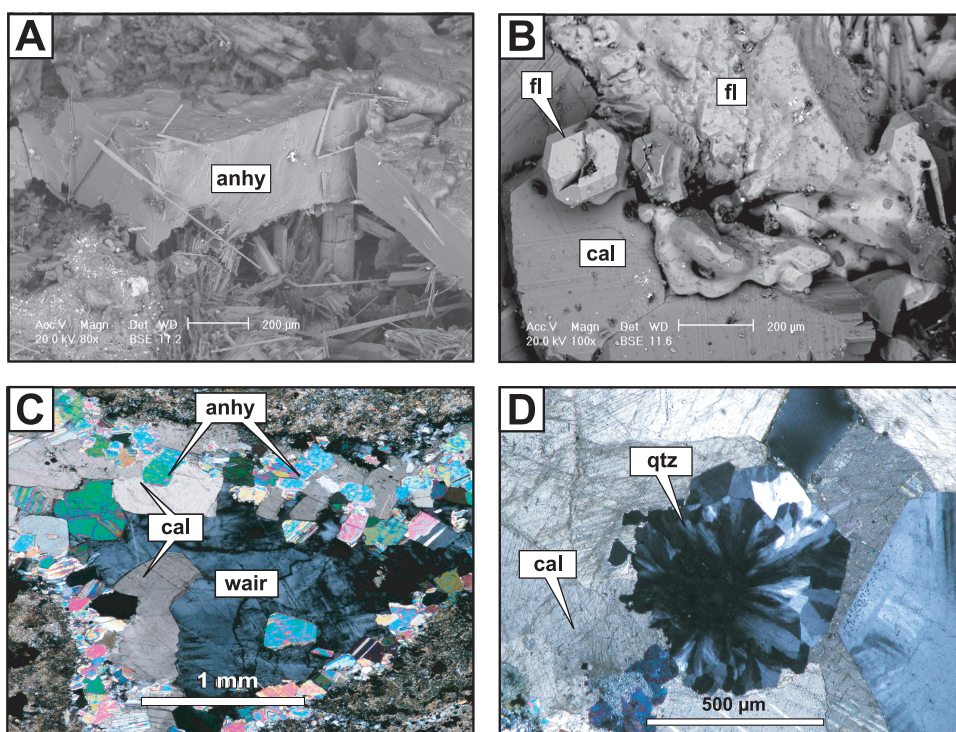
Fig. 12. Minerals and textural relationships typical of assemblage 3. (A) SEM back-scattered electron image of anhydrite encapsulating crystals of epidote and needles of actinolite. From 629 m elevation in T-8. (B) SEM back-scattered electron image of fluorite deposited on calcite. From 878 m elevation in T-2. (C) Wairakite after anhydrite and calcite. From -132 m elevation in K-21. Crossed nicols. (D) Quartz crystal formed during assemblage 2 encapsulated in assemblage 3 calcite. The complex extinction pattern is typical of assemblage 2 quartz. The irregular edges of the quartz crystal reflect dissolution by steam condensate. From 169 m elevation in K-33. Crossed nicols. Abbreviations: anhy = anhydrite; cal = calcite; fl = fluorite; qtz = quartz; wair = wairakite.

adjacent to the vein (epidote I) and a younger generation of acicular epidote (epidote II) deposited on the growing quartz crystal and subsequently encapsulated within it. Two generations of prehnite are shown in figure 13B. Prehnite I formed along the vein margin prior to quartz deposition; prehnite II defines a growth zone within the quartz crystal.

Less commonly, quartz is intergrown with calcite, wairakite and anhydrite, minerals typical of assemblage 3. In figure 13A, wairakite and calcite occur as both solid inclusions in the quartz and as later minerals that encapsulate the quartz crystal. Here, epidote occurs in an earlier growth zone. We interpret these relationships as indicating that growth of wairakite and calcite began during the deposition of assemblage 2 quartz and that the transition from assemblage 1 to 3 was relatively rapid.

Assemblage 3

Assemblage 3 is characterized by anhydrite, calcite and wairakite (fig. 12). In addition, Moore and others (2004a) assigned occurrences of alunite, natroalunite, kaolinite, pyrite, sepiolite and smectite, and the fluorite, native S and tourmaline present in the upper portion of T-2 to this assemblage. The alunite group minerals are commonly found as thin veins and as a replacement of plagioclase phenocrysts within
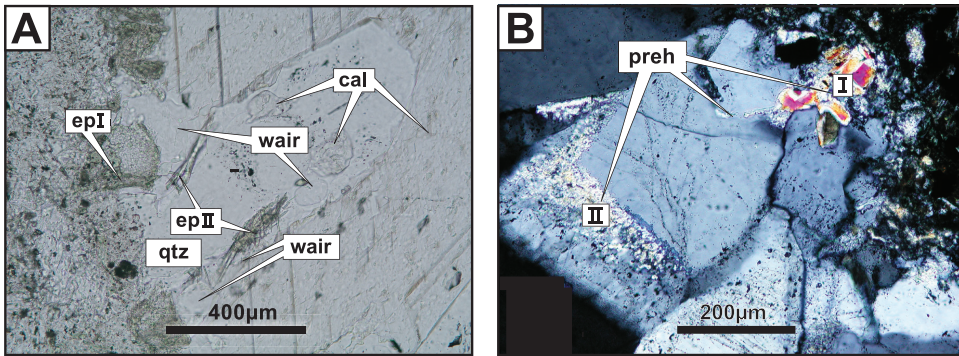
Fig. 13. Photomicrographs of transitional assemblages. (A) Vein quartz (representing assemblage 2) is intergrown with epidote, wairakite and calcite. Wairakite and calcite are representative of assemblage 3. Earlier epidote (ep 1) representing assemblage 1 occurs in the wall rock. Growth of wairakite and calcite continued after quartz deposition, filling the vein interior. From -222 m elevation in K-21. Plain light. (B) Quartz (representing assemblage 2) with growth zones outlined by prehnite. Prehnite, which formed late in the evolution of assemblage 1, was growing on the vein wall prior to quartz deposition. An older crystal of epidote lies beneath the quartz crystal. From 20 m elevation in K-33. Crossed nicols. Abbreviations: cal = calcite; ep = epidote; preh = prehnite; qtz = quartz; wair = wairakite.

the upper 340 m of the well, but persist locally to depths of 475 m. Between depths of ~350 and 750 m anhydrite is the common sulfate-bearing mineral. Pyrite fills veins that both predate and postdate anhydrite, although most of the coarse-grained pyrite is younger than anhydrite. Native S occurs sporadically between depths of 370 and 440 m. Between depths of 340 and 725 m, fine-grained needles and pale blue-green radiating aggregates of tourmaline are encapsulated in anhydrite and occasional contemporaneous quartz. Electron microprobe analyses of tourmaline from 634 m depth indicate it is a high alumina dravite containing only minor Ti and Fe in the Y-site. Calcite, and locally fluorite, is found below 700 m in this well.

The alunite group minerals are diagnostic of advanced argillic alteration and interactions with aggressive acid SO_4 water (Hemley and others, 1969, 1980). Moore and others (2004a) modeled these interactions at temperatures up to 250°C using the composition of acidic water from Telaga Bodas (table 2) and that of a typical andesite. It was assumed the water was conductively heated as it percolated downward from the lake. The simulations demonstrate that the mineral distributions observed in T-2 could be produced as the water was neutralized. They also predict a decrease in the freezing-point depressions of the fluid with increasing temperature, consistent with measurements on fluid inclusions trapped in anhydrite, calcite and fluorite described below. Advanced argillic alteration was not found in other wells, although it is likely that acid SO_4 water has produced comparable assemblages in the highly altered rocks at Kawah Karaha and possibly at depth within the magmatic vapor-dominated chimney.

At depth in T-2, and in other wells, anhydrite and/or calcite fill veins and encapsulate earlier formed minerals (fig. 12). Much of the anhydrite and calcite that replace feldspar phenocrysts in the deeper rocks, where these veins are found, may also have formed at this time.

Wairakite occurs as a replacement of the wall rock and as euhedral vein fillings, in places intergrown with chlorite. Wairakite encapsulates epidote, prehnite and quartz, demonstrating that the deposition of wairakite postdates these minerals. Although wairakite frequently occurs in rocks that also contain veins of anhydrite and calcite, textural relationships illustrated in figure 12C and crosscutting veins demonstrate that
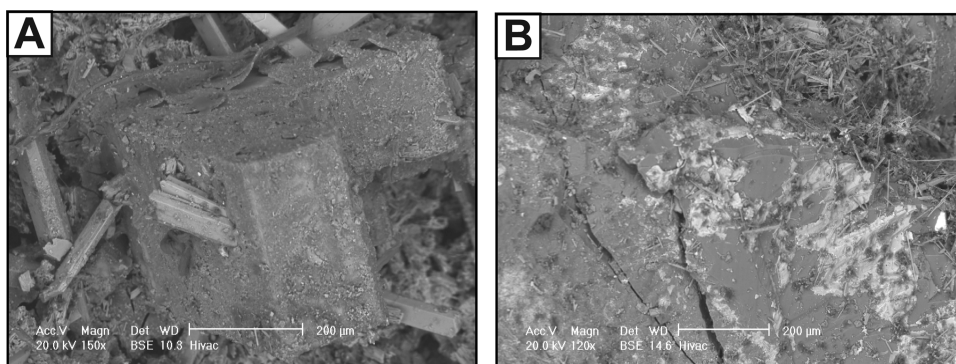
Fig. 14. SEM backscattered electron images of scale deposits. (A) Ti-rich precipitate coating anhydrite. The anhydrite encapsulates crystals of epidote. From 586 m elevation in T-8. Anhydrite from this depth contains vapor-rich and halite-saturated fluid inclusions. (B) White encrustations of FeCl$_x$ on quartz. From 461 m elevation in T-8.

their deposition was not contemporaneous. In figure 12C, intergrowths of calcite and anhydrite line the walls of a vug whose interior is filled with wairakite. These relationships indicate that wairakite was the last mineral deposited. Less commonly, wairakite occurs along the vein walls and is coated with later anhydrite and calcite.

Assemblage 4

A variety of scales coat the rock surfaces within the vapor-dominated region of the field. SEM EDS analyses of samples from T-2 and T-8 document precipitates of NaCl, KCl, FeCl$_x$ and Ti-Si-Fe (fig. 14), and X-ray diffraction analyses indicate halite. The high solubilities of these precipitates imply complete drying out of any inflowing liquid and residual pore fluids within the low-pressure, but high-temperature vapor-dominated zone.

FLUID-INCLUSIONS

Fluid inclusions were studied in quartz, calcite, anhydrite and fluorite. Measurements on quartz provide information on assemblage 2; those on calcite, anhydrite and fluorite document conditions associated with assemblage 3. Fluid inclusions in growth zones (primary inclusions) (figs. 15A and15B) and healed fractures (secondary or pseudosecondary inclusions; Roedder, 1984) (fig. 15C) were measured. Only measurements on liquid-rich inclusions from fluid inclusion assemblages with consistent homogenization temperatures (that is ~90% of the inclusions homogenized within a 20°C range; Bodnar and others, 1985; Goldstein and Reynolds, 1994) are reported. Fluid inclusion assemblages with homogenization temperatures falling substantially outside this range were considered to reflect the effects of post-entrapment changes (necking or leaking) or heterogeneous trapping of liquid and vapor. These assemblages are not reported.

Fluid Inclusions in Quartz (Assemblage 2)

Microthermometric measurements were performed on ~1800 quartz-hosted inclusions from more than 30 depth intervals in T-2, T-8, K-21 and K-33. With the exception of quartz from 529 m elevation in T-8, only two phase liquid and vapor-rich inclusions were observed. Fluid inclusions from this sample contain liquid, vapor and solid phases (figs. 15D and 15E).

Liquid- and vapor-rich inclusions were observed in nearly every quartz crystal studied, but typically not in the same fluid inclusion assemblage. Fluid inclusion assemblages
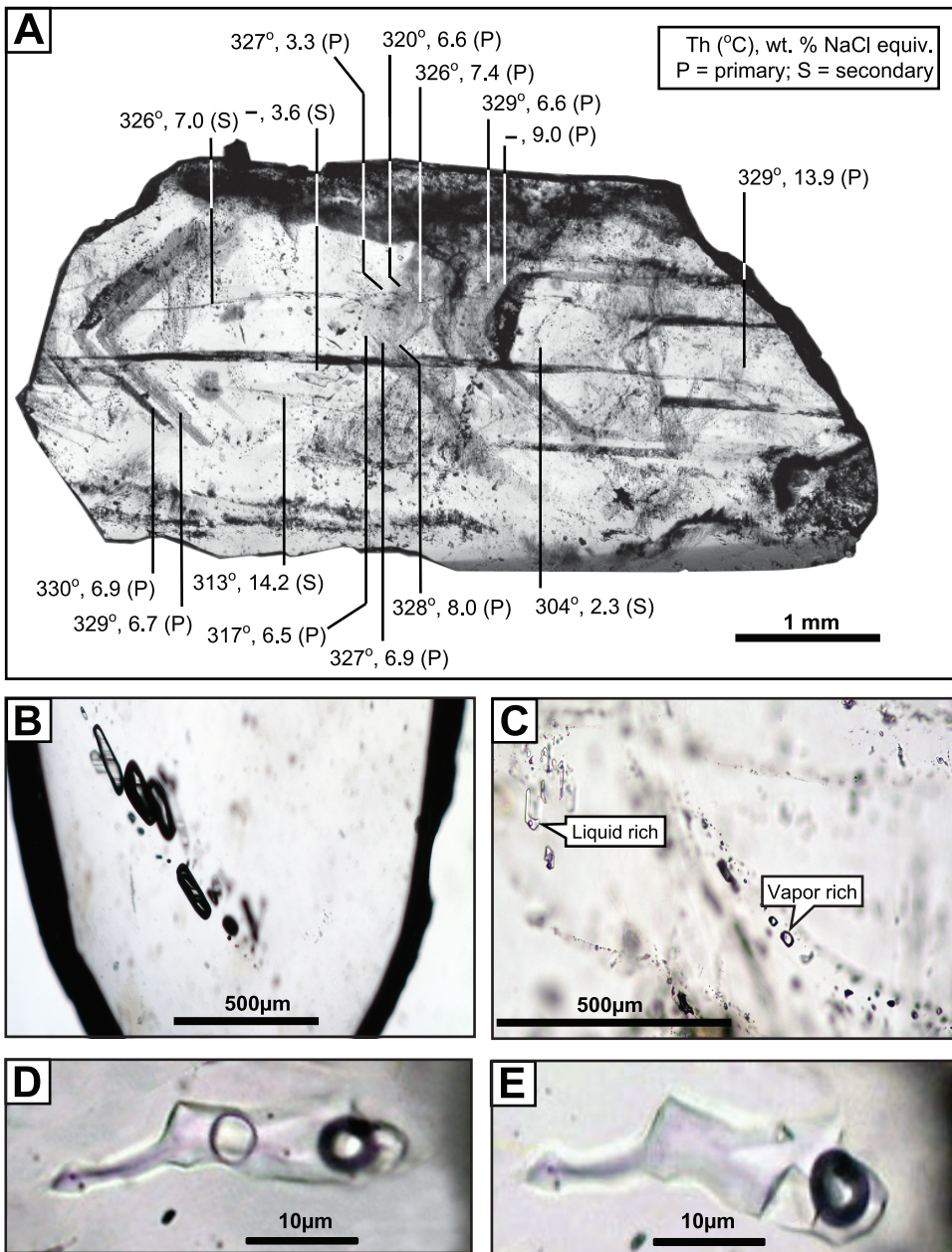
Fig. 15. Examples of fluid inclusion types. (A) Quartz crystal with fluid inclusions trapped in growth zones (primary inclusions (p)) and healed fractures (secondary inclusions (s)). The average homogenization temperature (Th) and salinity (in weight percent NaCl equivalent) are shown for each fluid inclusion assemblage. From 461 m elevation in T-8. (B) Growth zone in quartz defined by primary vapor-rich fluid inclusions trapped parallel to a rhombic face. From -222 m elevation in K-21. (C) Pseudosecondary inclusions trapped along healed fractures within a growth zone. Two fractures are labeled. One contains only liquid-rich inclusions; the other only vapor-rich inclusions. (D-E). A liquid-rich fluid inclusion containing a fluorite daughter crystal. From 528 m elevation in T-8. At room temperature, the fluorite forms a rounded crystal near the center of the inclusion (D). The octahedral crystal of fluorite adjacent to the vapor bubble formed when the inclusion was heated to a temperature slightly below the point of complete dissolution and then slowly cooled (E).

containing only vapor-rich inclusions indicate boiling has occurred, but not necessarily where the inclusions were trapped (Bodnar and others, 1985). However, boiling at the sample site can be inferred if it can be shown that liquid water was present.

Growth zones containing large primary vapor-rich inclusions are common in many samples (fig. 15B). Because liquid must have been present as the quartz crystals grew, these primary fluid inclusions are taken as evidence of boiling at the sample site. Healed fractures containing only vapor-rich inclusions occur in all wells but are most abundant in T-8. The presence of liquid water during the trapping of these inclusions is inferred from healed fractures containing liquid-rich inclusions within the same growth zone (pseudosecondary inclusions) (fig. 15C) and the deposition of quartz surrounding the growth zones.

Vapor-rich inclusions are rarely abundant in geothermal systems despite evidence of boiling from mineral assemblages, temperature – depth relationships, and fluid inclusion gas compositions (Browne and others, 1976; Roedder, 1984; Hedenquist and Henley, 1985; Hedenquist and others, 1992; Moore and others, 2000b). Bodnar and others (1985) suggested that the abundance of vapor-rich inclusions may reflect the degree of boiling, which can range from minor to flashing. Based on observations on samples from numerous other geothermal systems (unpublished data), the abundance of vapor-rich inclusions in all four core holes at Karaha – Telaga Bodas is interpreted to be the result of widespread flashing of the liquid. Moore and others (2000a) documented similar vapor-rich fluid inclusion assemblages in quartz from The Geysers. These inclusions were trapped when the early liquid-dominated system boiled off to form the modern vapor-dominated regime.

Liquid-rich fluid inclusions trapped in quartz record temperatures ranging from 123° to 348°C. The distribution of homogenization temperatures of individual fluid inclusion assemblages with respect to elevation and the measured downhole temperatures are plotted in figure 16. Because it can be inferred that the fluids were boiling at the time of quartz deposition, the homogenization temperatures of primary fluid inclusions, and possibly many of the secondary inclusions, represent the true trapping temperatures (Roedder and Bodnar, 1980).

Most samples in T-8 record paleotemperatures up to ~40° to 50°C higher than the present-day downhole conditions, whereas in K-21, the maximum homogenization temperatures frequently exceed the measured temperatures by 65° to 90°C. Only one sample from K-33 records paleotemperatures more than ~35°C higher than the downhole measurements. The differences between the modern and paleotemperatures suggest that the southern part of the field was hotter at the onset of quartz deposition than the central and northern parts, as they are today, and that the extent of cooling since quartz deposition was greatest in the north. In T-2 and the upper portion of K-21, homogenization temperatures commonly fall below the measured downhole temperatures. Thus the present-day conditions may record a thermal pulse occurring since quartz deposition.

Temperature-salinity relationships are shown in figure 17. The highest salinity fluids, ranging up to 26 weight percent NaCl-CaCl$_2$ equivalent, were trapped in quartz from T-8, although high salinities are also found in a sample from an intermediate depth in T-2. In contrast, salinities in K-21 and K-33 do not exceed ~2 weight percent NaCl equivalent.

Fluid temperatures and salinities varied during quartz deposition but not in a systematic manner. In the quartz crystal shown in figure 15A, primary fluid inclusions record salinities ranging from 3.3 to 13.9 weight percent NaCl equivalent and homogenization temperatures of 317 to 330°C. Secondary inclusions record similar ranges.

Quartz-hosted inclusions from 529 m elevation in T-8 contain up to six solid phases (figs. 15D and 15E). Fluorite, identified on the basis of its optical characteristics, is the most
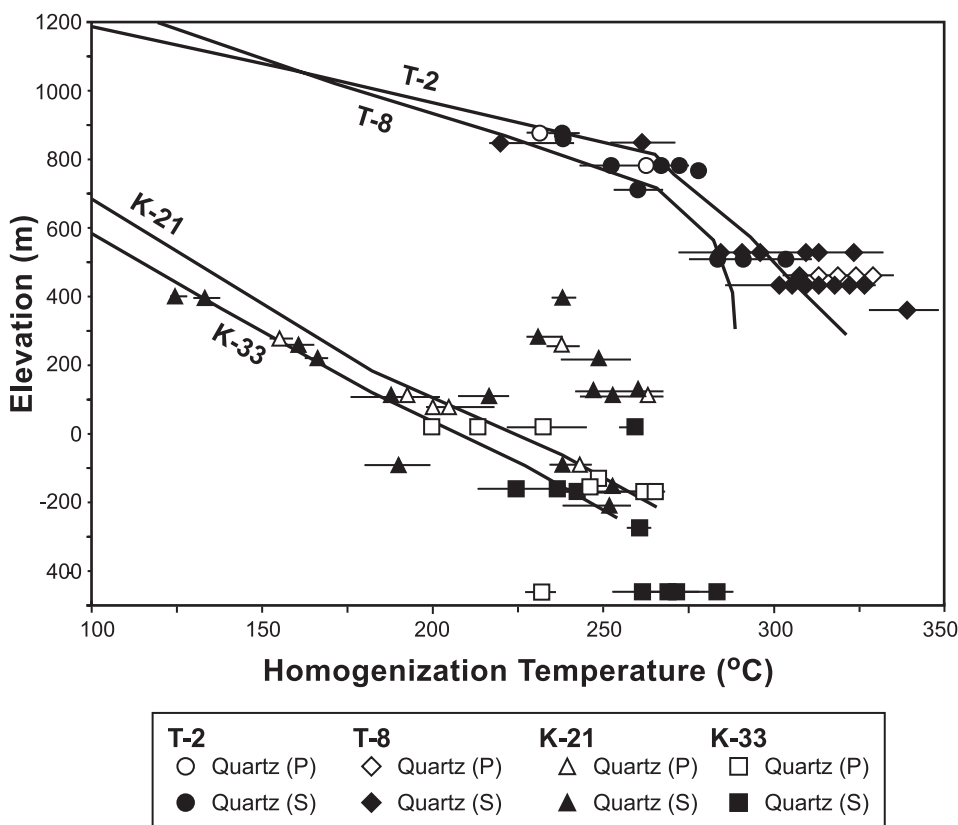
Fig. 16. Homogenization temperatures of fluid inclusions trapped in quartz (assemblage 2) from T-2, T-8, K-21 and K-33. The average homogenization temperature of each fluid inclusion assemblage is plotted. Horizontal lines represent the range of homogenization temperatures. Measured downhole temperatures are shown by solid lines.

common and in many inclusions the only daughter mineral present. Although the fluorite crystals form rounded grains at room temperature, octahedral crystals can be grown when the inclusions are slowly cooled from a temperature just below the point where dissolution is complete. Dissolution temperatures ranged from 254° to 313°C (n = 25). None of the other solid phases in the inclusions could be identified.

Fluid inclusions are present in chalcedony, but most are vapor-rich. However, even measurements on apparently primary liquid-rich inclusions in chalcedony may not yield data on the conditions at the time of mineral deposition because of post depositional recrystallization and maturation (Fournier, 1985; Sanders and Black, 1988). Fluid inclusions were however, measured in quartz crystals from two veins where botyroidal textures provide evidence of early chalcedony deposition. Primary inclusions in quartz from T-2 (878 m elevation) yielded homogenization temperatures of 228° to 234°C (average 232°C; n = 30) and an average salinity of 1.1 weight percent NaCl equivalent (n = 19). Secondary inclusions yielded a similar average homogenization temperature (235°C) and salinity (1.4 weight percent NaCl equivalent). Secondary fluid inclusions in quartz from T-8 (428 m elevation) yielded temperatures of 298° to 335°C (average 318°C; n = 73) and an average salinity of 18.4 weight percent NaCl equivalent (n = 27).
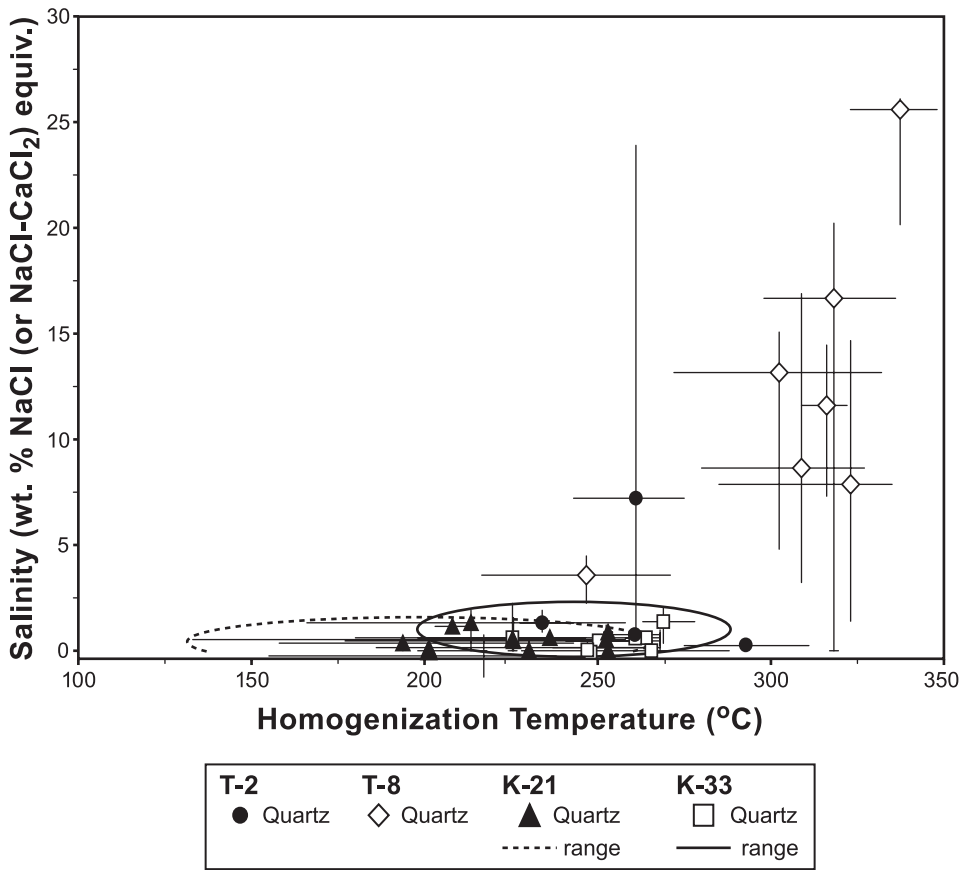
Fig. 17. Homogenization temperatures and salinities of fluid inclusions trapped in quartz (assemblage 2) from T-2, T-8, K-21 and K-33. The symbols show the average temperature and salinity of all inclusions in the sample. Horizontal lines represent the range of homogenization temperatures; vertical lines represent the range of salinities of samples from T-2 and T-8. Data for K-21 and K-33 plot within their respective ellipses. Salinities are expressed as either weight percent NaCl equivalent (salinities <23.2) or weight percent NaCl-CaCl$_2$ equivalent (salinities >23.2).

Fluid Inclusions in Anhydrite, Calcite and Fluorite (Assemblage 3)

Temperature-depth and temperature salinity relationships of fluid inclusion assemblages in anhydrite, calcite and fluorite from T-2, T-8, K-21 and K-33 are shown in figures 18 and 19 respectively. Two phase liquid-rich inclusions dominate, although both vapor rich and rarely three phase liquid-rich inclusions containing halite are present. Homogenization temperatures range from 108° to 308°C, and with few exceptions closely mimic the measured temperatures, suggesting recent trapping. In T-8, in contrast, the maximum homogenization temperatures of most samples signifi-cantly exceed the present-day conditions.

Fluid inclusions from T-2 and T-8 display a progressive change in their composition and temperature with depth (Moore and others, 2004a). As shown in figure 19, salinities initially decrease as temperatures increase to 205°C. The salinities then remain nearly constant as the homogenization temperatures increase further to 235°C. At this point, the trend reverses and the salinities increase with increasing temperature. The progressive decrease in salinity was attributed to the incorporation of SO$_4$ into the newly formed
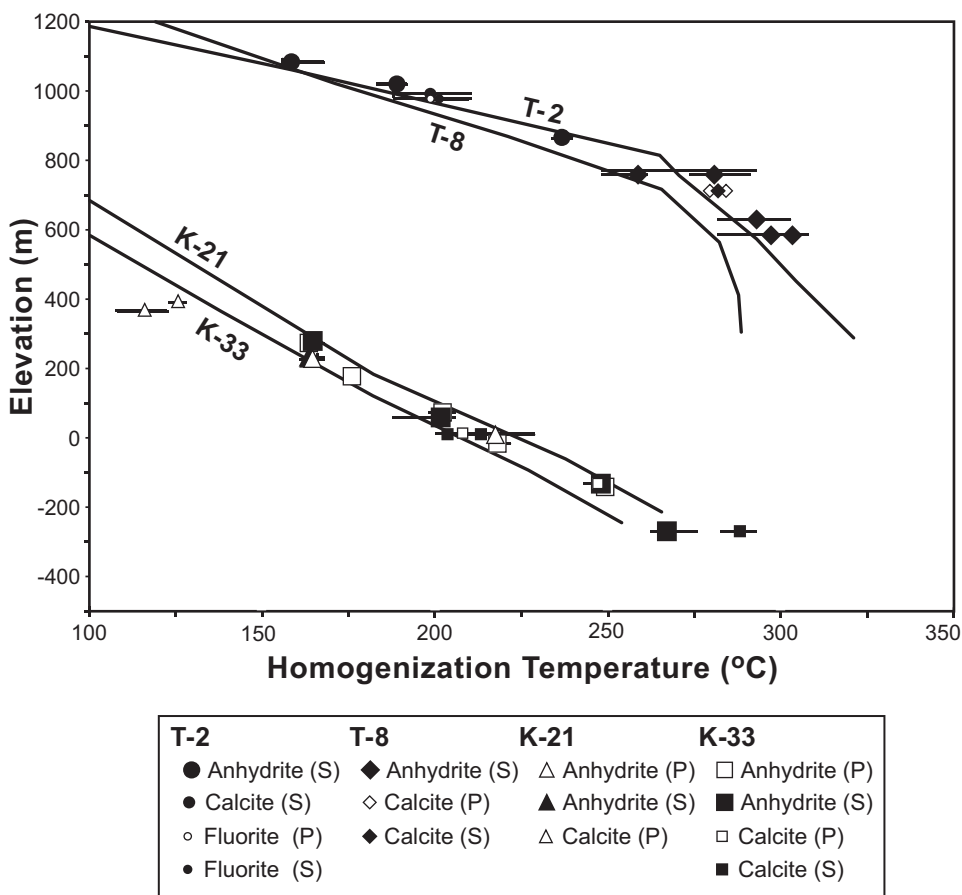
Fig. 18. Homogenization temperatures of fluid inclusions trapped in anhydrite, calcite and fluorite (assemblage 3) from T-2, T-8, K-21 and K-33. The average homogenization temperature of each fluid inclusion assemblage is plotted. Horizontal lines represent the range of homogenization temperatures. Measured downhole temperatures are shown by solid lines.

hydrothermal minerals. This mechanism does not, however, provide an explanation for the subsequent increase in salinity with increasing temperature as discussed below.

The highest salinities are found in anhydrite deposited near the top of the vapor-dominated zone (sample from 586 m elevation in T-8). Anhydrite from this depth is coated with Ti-rich precipitate (refer to fig. 14A). Both vapor-rich and three phase liquid-rich inclusions were trapped. The three-phase inclusions homogenize to the liquid phase by disappearance of the vapor bubble at temperatures ranging from 283° to 308°C (average 297°C; n = 18). Halite dissolution temperatures yield a salinity of 31 weight percent NaCl equivalent. Anhydrite is uncommon in the deeper samples from this well.

In contrast to inclusions from T-2 and T-8, the salinities of inclusions from K-21 and K-33 show little variation with depth or temperature. All but one inclusion yielded a salinity between 0.0 and 0.9 weight percent NaCl equivalent (n = 176). Salinities near 0.0 are typical of fluid inclusions that trap steam condensate (Moore and others, 2000a) and dilute meteoric water. The trapping of condensate is supported by occurrences of corroded quartz crystals (refer to fig. 12D). In actively convecting geothermal systems, fluids rapidly equilibrate with quartz within days to weeks (Rim-
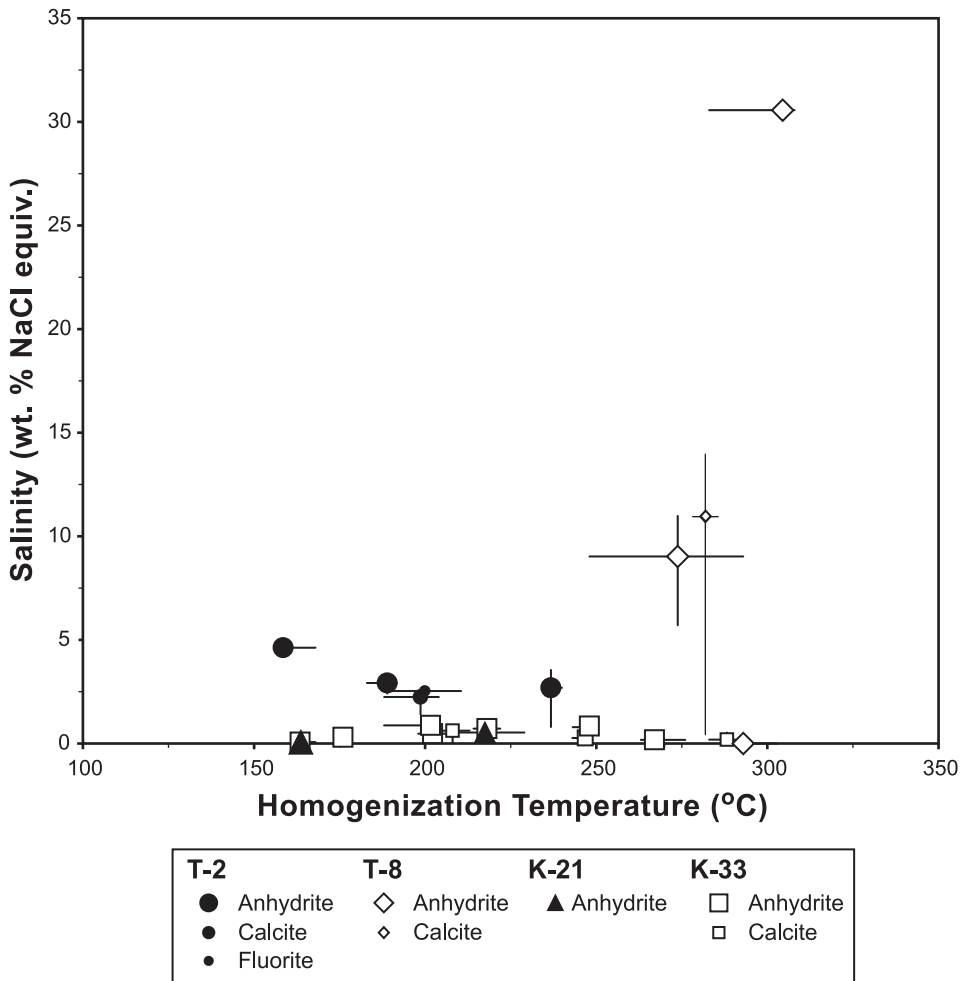
Fig. 19. Homogenization temperatures and salinities of fluid inclusions trapped in anhydrite, calcite and fluorite (assemblage 3) from T-2, T-8, K-21 and K-33. The symbols show the average temperature and salinity of all inclusions in the sample. Horizontal lines represent the range of homogenization temperatures; vertical lines represent the range of salinities. Salinities are expressed as weight percent NaCl equivalent. Inclusions with salinities of 31 weight percent NaCl equivalent are halite-saturated at room temperature.

stidt and Barnes, 1980). Thus, dissolution of quartz implies interactions with fluids whose circulation paths are relatively short. The relatively high homogenization temperatures of these inclusion fluids suggest they are more likely to represent low salinity steam condensate generated near the site of quartz dissolution than cool, rapidly descending shallow groundwater. Higher salinities, exceeding a few tenths weight percent, may reflect the effects of water-rock interactions, mixing with *in-situ* reservoir waters and the presence of dissolved gases (for example, Hedenquist and Henley, 1985).

DISCUSSION

The hydrothermal mineral assemblages, fluid inclusion measurements, ^{14}C ages of the lake beds, and present-day chemical, pressure and temperature data from Karaha – Telaga Bodas provide an unusually complete record of a rapidly evolving

volcanic-hosted geothermal system. In this section, we first summarize the evolution of the geothermal system. A general model of volcano-hosted vapor-dominated geothermal systems is then presented.

The earliest mineral assemblage, assemblage 1, documents the presence of a high-temperature liquid dominated system. The progressive appearance of smectite, mixed layer illite-smectite, illite, epidote, actinolite, biotite and tourmaline (fig. 9) indicate temperatures increase with depth. No fluid inclusion measurements were made on assemblage 1 minerals. However, the mineral assemblages suggest deposition from a near neutral NaCl water (Ellis and Mahon, 1977). Based on the composition of the fluids trapped in assemblage 2 quartz, the salinity of the circulating hydrothermal fluids may not have exceeded ~2 weight percent NaCl equivalent (see below).

Altered rocks containing biotite and tourmaline are relatively uncommon in geothermal systems, forming only in the contact regions of intrusions where temperatures exceed 300°C (Corbett and Leach, 1998). Thus the occurrence of these minerals in the northern part of the field is consistent with their formation during emplacement of the granodiorite. Although the continuity of the biotite and tourmaline surfaces from Kawah Karaha southward suggests the granodiorite forms an elongate stock beneath the axis of the volcanic ridge, it was not encountered in the deep drill holes near Telaga Bodas. Nevertheless, the high measured temperatures and paleotemperatures suggest that it must lie at relatively shallow depths beneath Telaga Bodas.

The transition from assemblage 1 to 2 is, in some samples, represented by intergrowths of epidote or prehnite with quartz. In the central part of the field, where both calc-silicate minerals are present, epidote is always found to be overgrown by prehnite. As shown in figure 20 (path A), the occurrence of prehnite after epidote indicates that temperatures had already begun to wane prior to the formation of assemblage 2 quartz.

The deposition of assemblage 2, represented by the silica polymorphs, records a change in the physical and chemical conditions. Within geothermal reservoirs, quartz controls dissolved silica at temperatures >180°C, whereas chalcedony controls silica at lower temperatures (Fournier, 1985). Consequently, chalcedony is rarely observed in the high temperature portions of active geothermal systems where propylitic assemblages dominate. The deposition of chalcedony within the propylitic zones at Bulalo, Philippines (Stimac and others, 2006), a liquid-dominated geothermal system, and at The Geysers, California (Moore and others, 2000a) are notable exceptions.

The deposition of chalcedony at temperatures >225°C at Karaha – Telaga Bodas, as indicated by fluid-inclusion measurements and the accompanying mineral assemblages, requires oversaturation of silica with respect to quartz. Similarly, the deposition of alternating bands of chalcedony and amorphous silica at lower temperatures implies oversaturation of silica with respect to chalcedony. Oversaturation can result from boiling or cooling. For a fluid in equilibrium with quartz at 225°C, only 14°C of cooling, assuming no steam loss, is necessary to saturate the fluid with respect to chalcedony. However, 103°C of cooling is required for a fluid in equilibrium with chalcedony at ~160°C (near the common upper temperature limit of this mineral) to become saturated with respect to amorphous silica (Fournier, 1981). Alternating bands of amorphous silica and chalcedony require repetitive episodes of heating and cooling (refer to fig. 11A). Such short-term temperature oscillations are unlikely and have not been documented in geothermal systems. Nor will cooling produce the fluid inclusion assemblages observed in the quartz crystals.

Boiling, in contrast, provides an explanation for the common occurrence of vapor-rich inclusions trapped in the quartz crystals. At 250°C, a fluid in equilibrium with quartz will become saturated with respect to chalcedony when 7 percent of the water is lost as steam. Mixing with water undersaturated with respect to chalcedony (for example steam condensate) will reestablish equilibrium with quartz. Similarly, fluids in equilibrium with
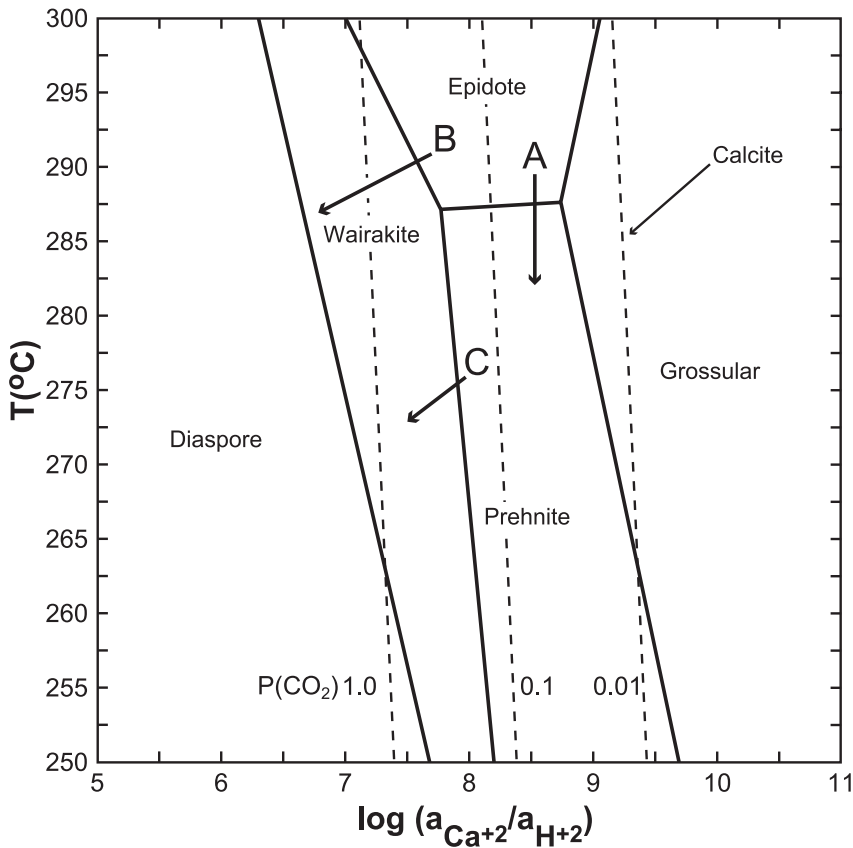
Fig. 20. Mineral stability relations in the system Ca-Fe-Al-Si-H_2O-Cl assuming equilibrium with quartz and pyrite, $f_{O2(g)} = 10^{-34}$ MPa and $a_{H2S(aq)} = 10^{-2.4}$, based on the composition of the reservoir fluid, and $a_{epidote} = 1$. Dotted lines show calcite stability at various CO_2 pressures. At P(CO_2) = 1 MPa, the epidote and most of the wairakite fields are covered by the "calcite blind". Quartz thermodynamic data from Fournier (1983); remaining data from Johnson and Lundeen (1994) with equilibrium constants of wairakite reduced by 0.6 log units to better represent commonly observed relations between wairakite and fluid chemistry in New Zealand geothermal systems (Bruton, 1995).

chalcedony at 160°C will become saturated with respect to amorphous silica when 70 percent of the fluid boils off. In this case, episodic boiling and inflow of low silica fluids can lead to the cyclic deposition of chalcedony and amorphous silica.

Boiling can occur in a closed (adiabatic) or open system. Although boiling is generally thought to occur under adiabatic conditions, open system boiling and steam loss can produce much greater compositional changes. For example, adiabatic boiling will only result in a 25 to 30 percent increase in salinity as the fluid boils from 300° to 100°C (Simmons and Browne, 1997). In contrast, boiling to near dryness can occur under open system conditions with little change in temperature. In low porosity rocks, significant dry-out can occur in response to a pressure drop of only a few tenths of a MPa (Grant and others, 1982).

Evidence of open system boiling is not commonly documented. Moore and others (2000a, 2000b) used the relative contents of CO_2, CH_4, and H_2 in fluid inclusions to demonstrate that open-system boiling occurred at The Geysers and at Tiwi, Philippines. Simmons and Browne (1997) concluded that open system boiling and vaporiza-

tion of more than 99 percent of the original liquid occurred locally during the deposition of sphalerite in the Broadlands - Ohaaki geothermal system, New Zealand. Carman (2003) proposed open-system boiling as the mechanism to explain the origin of salinities ranging from 5 to >40 weight percent NaCl equivalent in anhydrite-hosted inclusions from the Ladolam gold deposit on Lihir Island, Papua New Guinea. Here, the formation of hypersaline brines was attributed to dike emplacement and sector collapse of the volcano, which triggered decompression and widespread flashing of the fluid (Davies and Ballantyne, 1987; Moyle and others, 1990; Carman, 2003).

At Karaha – Telaga Bodas, the compositions of the liquid-rich fluid inclusions in T-2 and T-8 also vary widely, from 0 to 26 weight percent $NaCl$-$CaCl_2$ equivalent. These high salinities could result from open system boiling of an initially dilute reservoir fluid as discussed above. However, local enrichments in F (as fluorite) in fluid inclusions from T-8 imply the presence of a magmatic component (Corbett and Leach, 1998). This suggests the possibility that saline fluids derived from the underlying magma or generated during advanced argillic alteration on the margins of the vapor-dominated chimney by acid SO_4 waters were also trapped in the inclusions. Nevertheless, the common occurrence of vapor-rich inclusions and variations in the salinities of inclusion fluids trapped at similar temperatures only millimeters apart, as found in the quartz crystal shown in figure 15A, suggest that open system boiling was the dominant process controlling the fluid composi- tions. If the initial salinities of the inclusion fluids trapped in T-8 were comparable to the maximum salinities of those found in K-21, K-33, and most inclusions in T-2 (approxi- mately 2 weight percent NaCl equivalent), then the highest salinities in T-8 (26 weight percent $NaCl$-$CaCl_2$ equivalent) imply vaporization of ~ 94 percent of the water.

The deposition of chalcedony instead of quartz depends on the rate of quartz precipitation relative to the increase in silica concentration. Despite potentially high concentrations of silica resulting from open system boiling, chalcedony is only found at the base of the quartz crystals, or rarely, in T-8, as veins without euhedral quartz. Once chalcedony was deposited, quartz precipitation appears to have buffered subsequent increases in the silica contents, even though the common occurrence of vapor-rich inclusions indicates boiling continued. Taken together, these observations imply that the precipitation of chalcedony occurred early in the evolution of assemblage 2 in response to a hydrothermal event that resulted in fieldwide decompression, open- system boiling and the rapid escalation of silica concentrations.

The lake beds deposited at 5910 ± 76 years BP uniquely constrain the intrusive and hydrothermal history of the hydrothermal system. Rocks overlying the lake beds contain epidote and actinolite (assemblage 1) and later chalcedony and quartz (assemblage 2). The absence of multiple episodes of chalcedony deposition implies that individual eruptions of lava and pyroclastic flows were not responsible for fieldwide decompression of the thermal fluids. Instead, we suggest that widespread flashing of the early liquid system, and the development of the modern vapor- dominated regime, was triggered by the flank collapse that produced the volcano's crater, Kawah Galunggung, at 4200 ± 150 y BP (Bronto, ms, 1989). Emplacement of the granodiorite and deposition of alteration minerals representing assemblage 1 must therefore have occurred between ~6000 and 4200 years BP. Heat from still cooling portions of the granodiorite maintains the modern geothermal system.

Assuming two-phase conditions at the time of trapping, the homogenization temperatures and salinities from the inclusions can be combined to infer a fluid pressure. The inferred pressures with elevation (fig. 21) show two trends based on location. The southern, high temperature wells (T-2, T-8) follow a pressure trend that is close to a lithostatic gradient, and slightly below that inferred for a lithostatic gradient beneath Kawah Galunggung. This suggests that pressures within the volcanic system prior to the deposition of Assemblage 2 were very high, and close to the failure
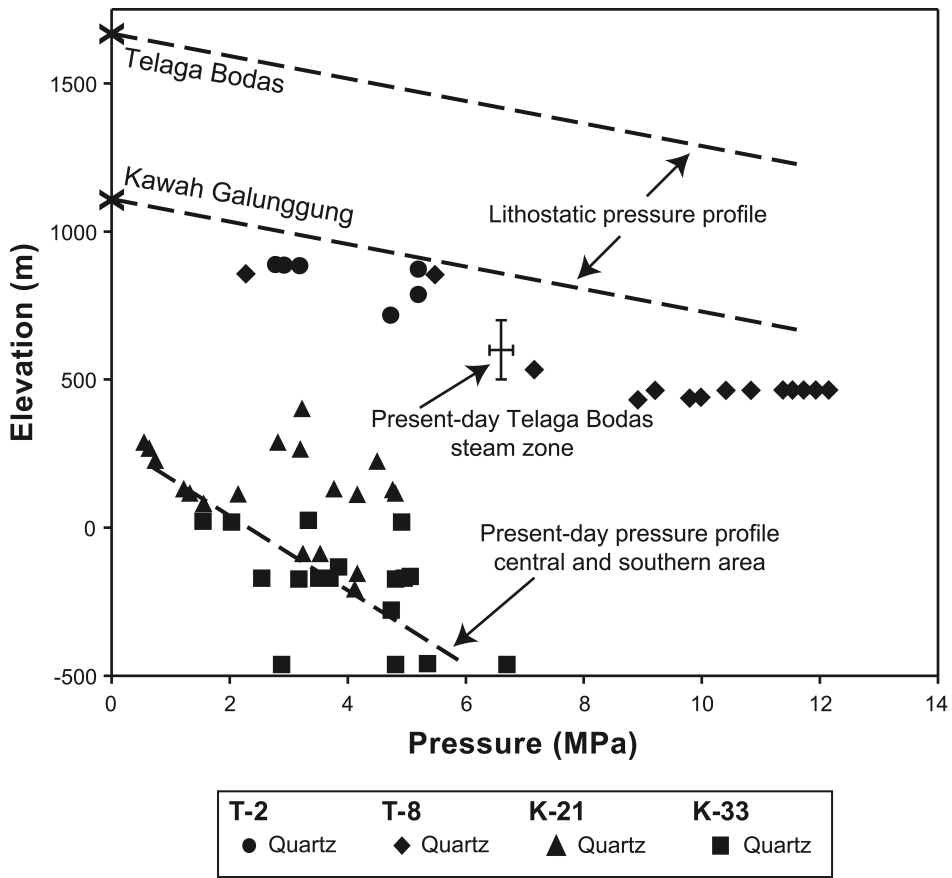
Fig. 21. Relationship between pressures calculated from the average homogenization temperature and salinity of each fluid inclusion assemblage and elevation. The pressures were calculated assuming that the fluid was boiling at the time the inclusions were trapped. For comparison with the fluid-inclusion data from T-2 and T-8, lithostatic pressure gradients beneath Kawah Galunggung on the volcanic flank and Telaga Bodas on the volcanic ridge are shown.

pressure around the flanks of the system. Ultimately, these high pressures may have triggered the flank collapse at Kawah Galunggung at ~4200 years BP. The inferred pressure trend in the central part of the field for most data is close to the present-day liquid pressures. Some evidence of higher pressures may reflect an earlier time when higher temperatures and/or liquid-dominated conditions existed, as noted earlier.

The deposition of quartz was followed by precipitation of vein calcite and anhydrite (assemblage 3). Anhydrite and calcite, in contrast to most silicate minerals, have retrograde solubilities. The progressive decrease in the salinities of anhydrite-, calcite- and fluorite-hosted fluid inclusions, as predicted by Moore and others (2004a), and absence of contemporaneous minerals with prograde solubilities in calcite and anhydrite veins suggests deposition occurred as descending SO_4- and CO_2-rich waters were heated (Simmons and others, 2000). The downward sealing of the marginal fractures by these minerals limited recharge, promoting continued growth of the vapor-dominated zone.

The increase in the salinities and temperatures of fluid inclusions trapped in T-8 (refer to fig. 19) at temperatures greater than 235ºC can also best be explained by open-system boiling of the steam-heated water as it migrated downward. This conclusion is supported by the abundance of vapor-rich inclusions and hypersaline fluids in
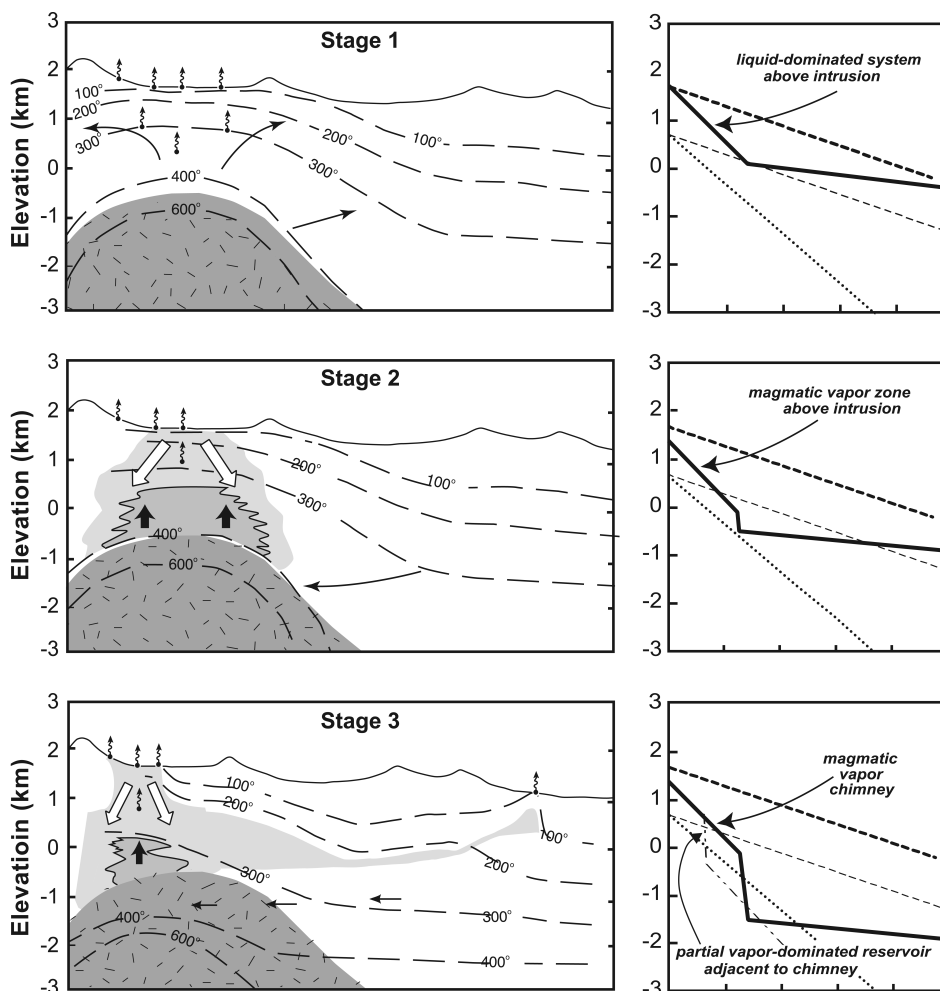
Fig. 22. Conceptual five stage model of the evolution of a vapor-dominated volcanic-hosted geothermal system. Stage 1 involves the formation of an over-pressured liquid-dominated geothermal system shortly after magmatic intrusion. High-temperature fumaroles could be present. In Stages 2 and 3, pressures progressively decrease, and a curtain of steam-heated water surrounding a magmatic vapor-dominated chimney at 350°C and 14 ± 2 MPa develops. The relatively low pressure near the base of the chimney leads to the development of a secondary marginal vapor-dominated zone. In Stage 4, both the magmatic vapor discharge and the vapor pressure decline. The secondary vapor-dominated zone expands above the intrusion. In Stage 5, the vapor-dominated zone floods because heat from the intrusion is insufficient to boil all liquid inflow, and a liquid-dominated volcanic-hosted system then develops.

anhydrite near the top of the vapor-dominated zone. Descending fluids that boiled dry deposited Na, K and Fe chlorides on the rock surfaces.

In the deep parts of the system, permeabilities were reduced by the deposition of wairakite. The common occurrence of wairakite in veins containing anhydrite and calcite are interpreted as indicating that wairakite deposition resulted from mixing of the reservoir fluids, with the descending slightly acidic water. Figure 20 (path B) shows that the formation of wairakite after epidote is favored by decreasing temperature and/or pH. This transition is typical of the southern part of the field. In the central and northern parts of the field, the formation of wairakite after prehnite at lower temperatures is attributed primarily to the decrease in fluid pH (path C).
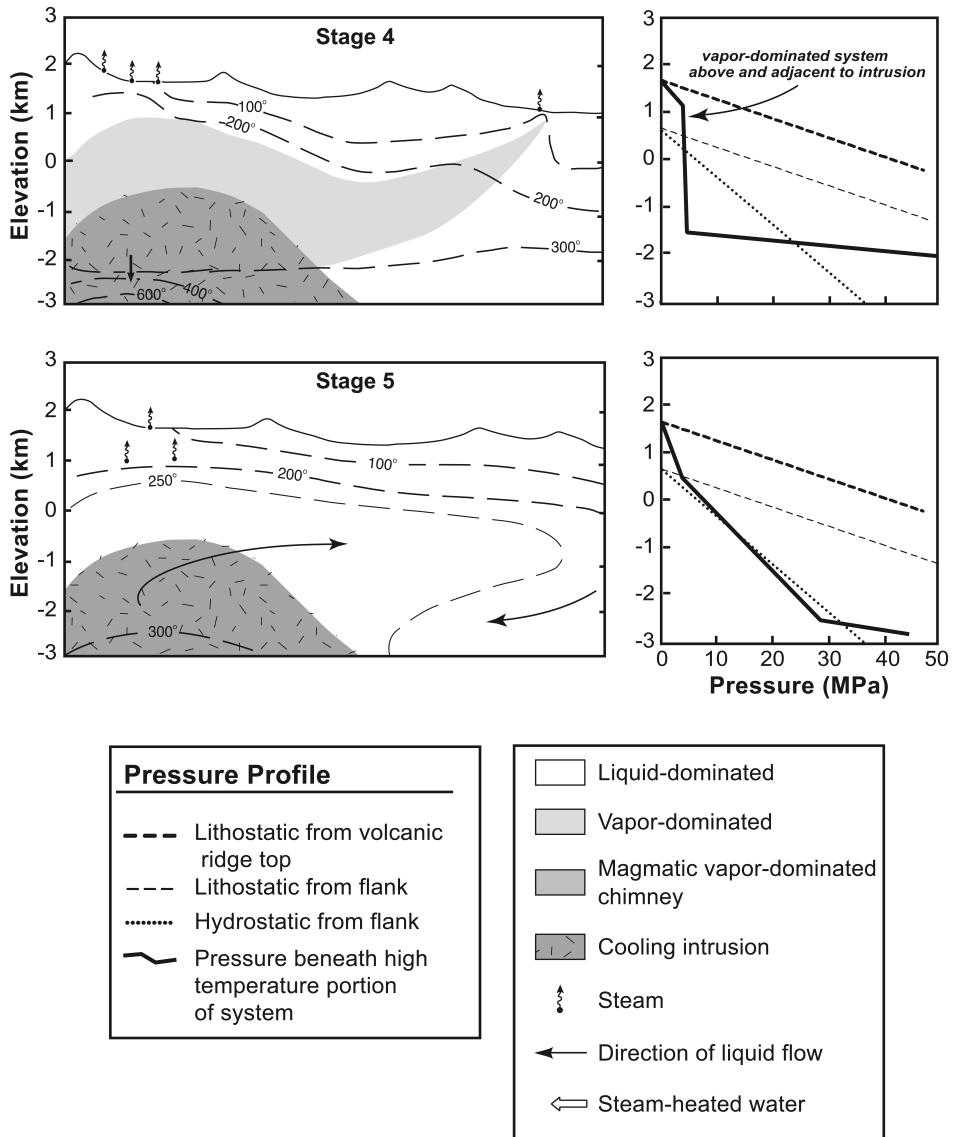
Fig. 22 (continued)

The modern reservoir fluids encountered beneath the vapor-dominated zone are low salinity meteoric and steam-heated waters derived from the ridge crest and possibly the adjacent valleys. This limited recharge is not sufficient to flood the vapor-dominated zone, although this will eventually happen. Stable isotopes suggest the modern geothermal fluids contain a significant magmatic component or that they interacted with young intrusive rocks. Gases in the north and south, while circulating long enough to come to chemical equilibrium with reactions involving H_2 and CO_2, have nonetheless failed to achieve equilibrium with H_2S and CH_4. Although the reservoir is in pressure communication along its length, heterogeneity in the liquid and gas chemistry across the field suggests that the system is composed of individual

cells in which the liquid chemistry is dictated by the Cl and B content of convecting steam. The effective base of the reservoir, represented by the transition from brittle to ductile deformational behavior, is predicted to lie near the top of the intrusion (Nemčok and others, 2003, 2006).

A Conceptual Model of Volcanic Hosted Vapor-Dominated Geothermal Systems

Vertically extensive vapor-dominated geothermal systems are hydrologically unstable and prone to flooding. Thus they must represent a transient state in the development of volcanic hosted systems. In this section, pressure and temperature relationships from Karaha-Telaga Bodas are combined with those from systems that contain only liquid- or vapor-dominated reservoirs to describe the evolutionary changes volcanic-hosted systems can undergo. This model expands on the concept of a vapor-dominated chimney in a cooling volcano proposed by Reyes and others (1993) to describe the characteristics of the Alto Peak, Philippines, geothermal system. They suggested the vapor-dominated chimney is initially at relatively high pressure with steam pressures slightly exceeding the adjacent liquid pressures (analogous to Model III of Ingebritsen and Sorey, 1988).

The evolutionary model we propose is subdivided into five stages, illustrated by the temperature-pressure relationships shown in figure 22. The model assumes that the brittle-ductile transition occurs between 350° and 400°C, as suggested by Fournier (1999). Permeabilities within the ductile zone are very low, and consequently, the thermal regime becomes predominantly conductive. Pressures within the ductile zone approach lithostatic values. The five stages are distinguished by a progressive deepening of the brittle-ductile transition within the cooling intrusion and by changes in the permeability and flow regime within the volcano due to fluid-rock interactions. Fluid flow at Karaha-Telaga Bodas appears to be essentially two dimensional and dominantly fault controlled at depth. Flow through porous volcaniclastic deposits occurs locally (Nemčok and others, 2004), but overall, intergranular porosity appears to be relatively low.

Stage 1.—The first stage is initiated by intrusion of a magma body into the base of the volcanic cone, possibly to depths of less than 2 km beneath the summit. This stage could be accompanied by volcanic eruptions and high-temperature fumaroles at ~800°C that discharge magmatic gases (Giggenbach, 1997; Hedenquist, 1998). Both the intrusive mass and the thermal effects on the pre-existing fluids in the overlying cone may be sufficient to cause strong over-pressuring. A liquid-dominated, probably gassy, geothermal system is assumed to form immediately above the intrusion (Fournier, 1999). High-salinity magmatic fluids characterize the ductile zone (Moore and Gunderson, 1995; Fournier, 1999; Hedenquist and others, 1999), pressures are lithostatic, and fluid flow is outwards from the intrusion. In the case of Karaha – Telaga Bodas, the initial pressure was ~10 MPa above the regional hydrologic regime beneath the flanks of the volcano, and was theoretically sufficient to produce hot springs near the summit of the volcano. There is no evidence, however, that such hot spring activity actually occurred.

Stage 1 may be relatively short-lived because of the magnitude of over-pressuring. Hydrofracturing on the flanks of the volcano is likely. This will have the effect of increasing the circulation volume of the system, although these increases will be tempered by boiling and permeability reductions due to mineral sealing. Fracturing will also lead to a change in the dominant flow paths, and a decrease in both fluid pressure and salinity. There is a high risk during this stage of massive volcano flank failure. Flank or summit failure at the time of intrusion is not uncommon (for example Mt. St. Helens) and is caused by lithostatic pressures in the rising magma exceeding the confining load of the volcanic cone. Massive slope failure could be also be triggered soon after emplacement of the intrusion by the increase in geothermal fluid pressure in the overlying pore water (Reid, 2004).

Although this over-pressured, liquid-dominated stage may evolve quickly, the alteration characteristics of Karaha – Telaga Bodas suggests that it must be long enough for a propylitic and biotite zone imprint to develop on the host rocks

surrounding the intrusion beyond the zone of ductile deformation. At Karaha – Telaga Bodas, the duration of propylitic alteration is bracketed by the ages of the 5910 ± 76 year old lake beds, and depressurization causing dry-out of the fluid system associated with flank collapse at 4200 ± 150 y BP (Bronto, ms, 1989).

Stage 2.—Stage 2 is marked by a change from predominantly liquid upflow in the brittle region above the intrusion to vapor upflow. Close to the intrusion the vapor could be superheated. At this stage, the width of the magmatic vapor-dominated zone may exceed its height. Steam-heated water forms above and marginal to the vapor-dominated zone. Acid fluids produced by the disproportionation of magmatic SO_2 to H_2S and H_2SO_4 result in intense alteration of the country rock. High fluid salinities develop near the site of acid generation as a result of interactions with the country rocks, rather than the more common NaCl waters characteristic of liquid-dominated geothermal systems, and contribute to the complex chemistry of Telaga Bodas waters. Such high salinity fluid is a likely candidate to explain the low resistivity of the inferred magmatic chimney depicted in figure 2. The pressure of the vapor-dominated zone could be ~14 ± 2 MPa, consistent with a temperature of 350°C and two phase, saline conditions (Haas, 1971; Fournier, 1999). Steam-heated waters enriched in SO_4 and CO_2 form above the vapor-dominated zone and drain back down into the reservoir and laterally away from the intrusion as outflow plumes. These downflow channels seal up rapidly with calcite and anhydrite because of their retrograde solubilities. The pressure gradient in the steam-heated water above the vapor-dominated zone is close to hydrostatic, apart from local fractures that allow upflowing vapor to reach the surface. The vapor-dominated zone pressure of ~14 ± 2 MPa implies a thickness of the hydrologic cap of ~1500 m. The pressure balance means that major hydrothermal eruptions are possible if the steam-heated water locally drains and allows the vapor-dominated zone to migrate to higher levels within the cone, or if the vapor pressure increases rapidly as a result of new intrusive pulses.

Water adjacent to the intrusion near the base of the vapor-dominated zone flows towards the intrusion and totally boils. Fluid pressures here are below the regional hydrologic pressures beneath the volcano flanks. The permeability in the basement and volcanic rocks adjacent to the intrusion determines the longevity of the magmatic vapor-dominated zone. High permeability due to active cross-cutting faults may mean the vapor-dominated zone is short-lived and the geothermal system rapidly floods and moves to Stage 5. In contrast to Stage 3, the only exploitable (that is predominantly non-magmatic fluid) resources that develop at this stage may be restricted to the outflow plumes of steam-heated water.

Stage 3.—In Stage 3, the magmatic vapor-dominated zone extends to greater depth as cooling causes the brittle - ductile transition to recede into the intrusive rocks. The vapor-dominated zone is at least 1 to 2 km in vertical extent. The shape of the vapor-dominated zone could resemble a chimney. Pressures in the vapor-dominated zone remain at ~14 ± 2 MPa and the vapor compositions still have a strong magmatic component. The surrounding "curtain" of steam-heated water and fracture sealing by calcite and anhydrite extends to greater depth.

The presence of low fluid pressures near the base of the vapor-dominated chimney has now caused a significant pressure decline in adjacent parts of the volcano that are in pressure communication. Where temperatures are high enough, a secondary, marginal vapor-dominated zone forms over the under-pressured deep liquid zone. This secondary vapor-dominated zone has few magmatic signatures when compared to the vapor-dominated chimney above the intrusion. Karaha–Telaga Bodas, Indonesia has evolved to this stage.

Stage 4.—Further cooling of the intrusion and recession of the brittle - ductile transition increases permeability with depth. Flow of magmatic gases declines due to a decreased volatile flux from the nearly crystallized magma. Pressures and temperatures in

the vapor-dominated chimney decline. The secondary vapor-dominated zone that developed in Stage 3 now expands into the original vapor-dominated chimney and most of the earlier steam-heated water drains towards the base of the vapor-dominated zone and boils. Inflows to under-pressured regions of the volcano result in the continued deposition of calcite and anhydrite and self-sealing around much of the geothermal system. All liquid inflow is boiled to dryness at the bottom of the system. The geothermal fields at Kamojang and Darajat, West Java Indonesia are at this stage. These vapor-dominated reservoirs have relatively low pressures (3.5 – 4.5 MPa). The deepest wells, which have been drilled to depths of up to −500 m elevation have not encountered an underlying liquid reservoir.

Stage 5.—In stage 5, the heat flux from the intrusion is finally insufficient to boil all meteoric inflows to the highly under-pressured geothermal system, and flooding occurs. The influx of meteoric waters into the vapor-dominated zone may be triggered by tectonic activity that ruptures the low-permeability boundary seal. The transition between Stages 4 and 5 could be relatively rapid. The increased liquid pressure at the base of the system quenches further boiling leading to a decrease in the rate of steam loss. Although the reservoir could undergo a temporary period of cooling and diminished thermal activity, the large increase in fluid pressure at the base of the Stage 4 vapor-dominated zone may trigger new hydrofracturing and enhanced water flow into hotter rock. Once liquid pressures come into balance with the regional hydrologic regime, pressures would stabilize. Upwelling of liquid accompanied by boiling at shallow depth is possible, and an outflow plume through the volcano's flank may develop. The hydrologic head of the upflow zone may not be far above the regional groundwater level, and may be controlled by the elevation of the outflow plume. The salinity of the reservoir will be less than a few weight percent, reflecting interactions between meteoric waters and the country rock at moderate temperatures. Most of the world's producing volcanic-hosted geothermal systems have reached this stage. They include, among others, Bulalo and Tongonan, Philippines (Abrigo and others, 2004; Salonga and others, 2004; Gonzalez and others, 2005), Awibengkok, Indonesia (Allis, 1999), and Hatchobaru and Kakkonda, Japan (Fujikawa and Ikegami, 1992; Shimada and Fujino, 1995; Tamanyu and Fujimoto, 2005).

CONCLUSIONS

Observations from the Karaha – Telaga Bodas geothermal system documenting progressive, near-isothermal decompression have been used to develop a conceptual evolutionary model of volcano-hosted vapor-dominated geothermal systems such as those found in West Java, Indonesia. The evolution of these systems is initiated with the emplacement of a shallow magma body into the volcanic cone. An over-pressured liquid-dominated system may develop quickly, leading to flank collapse and formation of a magmatic vapor-dominated chimney with temperatures of ∼350°C and pressures of 14 ± 2 MPa. These conditions occur just above the brittle – ductile transition. Where the magmatic vapor-dominated chimney can be sustained, intense rock alteration by acidic waters surrounding the chimney occurs. Telaga Bodas may overlie a relatively long-lived vapor-dominated chimney. The catastrophic depressurization and boiling triggered by the flank collapse is represented in the surrounding rocks by the deposition of chalcedony and then quartz, which contains abundant vapor-rich fluid inclusions. Steam-heated waters enriched in SO_4 and CO_2 form around the vapor-dominated zone and drain downward, sealing the fractures with anhydrite and calcite.

As pressures and temperatures progressively decline, the brittle-ductile transition recedes downward. The vapor-dominated magmatic chimney collapses and is replaced by a lower pressure vapor-dominated reservoir with few magmatic signatures, which is under-pressured with respect to the regional ground water surrounding the volcano. Sealing of marginal fractures by anhydrite and calcite expands downward, further limiting recharge by meteoric waters, and promoting expansion of the vapor-dominated zone.

Vapor-dominated conditions at Kamojang and Darajat, West Java, extend beyond the drilled depths.

When the deep heat source is unable to boil all liquid draining into the system, the vapor-dominated zone slowly floods, becoming progressively more liquid-dominated. Eventually the reservoir comes into pressure equilibrium with the regional hydrologic system and its characteristics resemble those in classic, liquid-dominated volcano-hosted systems of Indonesia, the Philippines and Japan.

The effective base of the geothermal reservoirs is controlled by the depth to the transition from brittle to ductile behavior (Fournier, 1999). Permeabilities within the ductile zone, where temperatures reach 350 to 400°C are very low. Consequently the deep thermal regime becomes predominantly conductive and the pressure profile trends towards the lithostatic load. The five stages in the evolution of these volcanic-hosted systems are distinguished by a progressive deepening of the brittle – ductile transition within the cooling intrusion and by changes in the permeability and flow regime within the volcano due to fluid-rock interactions.

APPENDIX 1

Well test data

Sample[*]	Date	Well Head Pressure (MPa g)	Total Mass Flow (kg/s)	Enthalpy (J/g)	Stm Frac (%)[¥]	Flow Duration (days)
K-33a	12/1/97	0.53	3.3	1492	48	1.0
K-33b	12/1/97	0.53	3.3	1492	48	1.0
KRH 2-1 RD	6/12/97	0.08			31	0.7
KRH 3-1 STb	6/14/97	0.34	31	1398	44	2.1
KRH 4-1a	8/31/97	1.10	30	2283	83	8
KRH 4-1b	9/4/97	2.52	25	2330	85	12
KRH 4-1c	9/13/97	1.41	33	2237	81	21
KRH 5-1a	9/25/97	0.66	12	1584	52	2
KRH 5-1b	10/2/97	0.45	10	1771	60	7
KRH 5-1c	12/17/97	0.58	25	1398	44	12
TLG 3-1a	2/17/98	0.82	18	2540	94	2
TLG 3-1b	2/18/98	0.81	16	2586	96	3
TLG 3-1c	2/20/98	0.74	16	2586	96	5
TLG 3-1d	2/23/98	0.72	15	2563	95	8

[*]Multiple samples are labeled alphabetically. [¥]Steam fraction

APPENDIX 2

Weirbox compositions of well waters

Sample*	Date	Na	K	Ca	Mg	Li	Fe	B	SiO$_2$	Al	As	Cl	F	SO$_4$	HCO$_3$	NH$_3$
K-33a	12/1/97	207	52	7	0.51	0.16	0.55	4.64	405	2.77	0.07	52	0.22	85.0	494	32.5
K-33b	12/1/97	197	50	6	1.11	0.19	4.00	4.4	490	3.20	<0.50	56	0.20	125	450	39.9
KRH 2-1 RD	6/12/97	573	70	5	0.42	0.98	2.47	44.6	471	0.59	1.52	722	1.45	172	265	6.76
KRH 3-1 STb	6/14/97	759	146	4	0.03	2.56	<0.5	66.3	826	0.45	2.49	1261	0.85	89.3	99.0	3.49
KRH 4-1a	8/31/97	2345	359	44	0.07	6.82	0.19	189	699			4012	<2.13	51.4	165	19.6
KRH 4-1b	9/4/97	2383	359	46	<0.01	6.69	<0.2	197	695			4014	<1.96	50.5	160	24.2
KRH 4-1c	9/13/97	2483	400	74	0.37	7.07	<0.2	191	699	0.53	13.4	4261	<1.98	38.0	127	22.6
KRH 5-1a	9/25/97	4851	1353	1097	1.49	39.4	0.41	167	179	0.16	16.2	11235	5.88	32.3	41.8	18.9
KRH 5-1b	10/2/97	4930	1652	1200	1.71	29.7	<0.21	1.73	873	<0.21	13.4	11594	3.65	22.8	50.9	19.7
KRH 5-1c	12/17/97	5675	1710	1487	3.70	31.3	3.60	207	112	0.40	15.2	12852	1.50	5.8	<5	42
TLG 3-1a	2/17/98	1813	264	110	0.02	0.62	0.75	389	1181	0.13	24.1	3094	6.34	185	171	8.09
TLG 3-1b	2/18/98	2032	305	235	0.06	0.85	0.20	574	449	0.05	33.7	3705	7.88	240	171	13.5
TLG 3-1c	2/20/98	2330	363	432	0.08	1.05	0.60	435	563	0.14	31.0	4663	9.83	152	161	19.5
TLG 3-1d	2/23/98	2207	366	527	0.07	0.97	0.52	842	1178	0.22	48.5	4612	10.68	126	144	19.2

Analytical values in mg/L. See table 1 for sample pH. *Multiple samples are labeled alphabetically

REFERENCES

Abrigo, Ma., Fe., V., Molling, P. A., and Acuna, J. A., 2004, Determination of recharge and cooling rates using geochemical constraints at the Mak-Ban (Bulalo) geothermal reservoir, Philippines *in* Ogena, M., Salonga, N., Stimac, J., and Moore, J., editors, Philippine Geothermal Systems: Response to Production: Geothermics, v. 33, p. 11–36.

Allis, R. G., 1999, Present-day hydrothermal conditions in the vicinity of Awi 1-2, Awibengkok geothermal field, Indonesia: Geothermal Resources Council Transactions, v. 23, p. 3–8.

Allis, R., Moore, J., McCulloch, J., Petty, S., and DeRocher, T., 2000, Karaha-Telaga Bodas, Indonesia: a partially vapor-dominated geothermal system: Geothermal Resources Council Transactions, v. 24, p. 217–222.

Anderson, E., Crosby, D., and Ussher, G., 2000, Bulls-eye? – Simple resistivity imaging to reliably locate the geothermal reservoir: Beppu, Japan, Proceedings World Geothermal Congress, p. 909–914.

Arnórsson S., and Gunnlaugsson, E., 1985, New gas geothermometers for geothermal exploration: Geochimica et Cosmochimica Acta, v. 49, p. 1307–1325.

Arribas, A., Jr., 1995, Characteristics of high-sulfidation epithermal deposits and their relation to magmatic fluid *in* Thompson, J. H. F., editor, Magmas, Fluids and Ore Deposits: Mineralogical Association of Canada Short Course Series, v. 23, p. 419–454.

Asrizal, M., Hadi, J., Bahar, A., and Sihombing, J. M., 2006, Uncertainty quantification by using stochastic approach in pore volume calculation, Wayang Windu Geothermal Field, W. Java, Indonesia: Stanford, California, Stanford University, Proceedings 31st Workshop on Geothermal Reservoir Engineering, p. 235–242.

Bethke, P. M., 1984, Controls on base and precious metal mineralization in deeper epithermal environments: United States Geological Survey Open File Report 84–890, 38 p.

Bodnar, R. J., 1993, Revised equation and table for determining the freezing-point depression of H_2O-NaCl solutions: Geochimica et Cosmochimica Acta, v. 57, p. 683–684.

Bodnar, R. J., Reynolds, T. J., and Kuehn, C. A., 1985, Fluid inclusion systematics in epithermal systems *in* Berger, B. R., and Bethke, P. M., editors, Geology and Geochemistry of Epithermal Systems: Reviews in Economic Geology, v. 2, p. 73–97.

Bogie, I., and MacKenzie, K. M., 1998, The application of a volcanic facies model to an andesitic stratovolcano hosted geothermal system at Wayang Windu, Java, Indonesia: Auckland, New Zealand, Proceedings 20th New Zealand Geothermal Workshop, p. 265–270.

Bronto, S., ms, 1989, Volcanic geology of Galunggung, West Java, Indonesia: New Zealand, University of Canterbury, Ph. D. thesis, 415 p.

Browne, P. R. L., 1978, Hydrothermal alteration in active geothermal fields: Annual Reviews in Earth and Planetary Science, v. 6, p. 229–250.

Browne, P. R. L., Roedder, E., and Wodzicki, A., 1976, Comparative study of past and present geothermal waters, from a study of fluid inclusions, Broadlands field, New Zealand: Prague, Proceedings of the International Symposium on Water-Rock Interaction, 1974, p. 140-149.

Bruton, C. J., 1995, Testing EQ3/6 and GEMBOCHS using fluid-mineral equilibria in the Wairakei geothermal system: Lawrence Livermore National Laboratory Report UCRL-ID-129280, p. 23.

Budhitrisna, T., 1986, Geologic map of the Tasikmalaya Quadrangle, West Java: Geological Research and Development Centre scale 1:100,000.

Carman, G. D., 2003, Geology, mineralization, and hydrothermal evolution of the Ladolam gold deposit, Lihir Island, Papua New Guinea *in* Simmons, S. F., and Graham, I., editors, Volcanic, Geothermal, and Ore-Forming Fluids: Rulers and Witnesses of Processes within the Earth: Society of Economic Geologists, Special Publication 10, p. 247–284.

Cavarretta, G., and Puxeddu, M., 1990, Schorl-dravite-ferridravite tourmaline deposited by hydrothermal magmatic fluids during early evolution of the Larderello geothermal field, Italy: Economic Geology, v. 85, p. 1236–1251.

Corbett, G. J., and Leach, T. M., 1998, Southwest Pacific Rim Gold-Copper Systems: Structure, Alteration and Mineralization: Society of Economic Geologists Special Publication Number 6, 237 p.

Craig, H., 1963, The isotope geochemistry of water and carbon in geothermal areas, *in* Tongiorgi, E., editor, Nuclear Geology in Geothermal Areas: Pisa, Italy: Consiglio Nazionalle delle Ricerche, Laboratorio de Geologia Nucleare, p. 17–53.

Cumming, W., and Mackie, R., 2007, 3D MT resistivity imaging for geothermal resource assessment and environmental mitigation at the Glass Mountain KGRA, California: Geothermal Resources Council Transactions, v. 31.

Cumming, W., Nordquist, G., and Astra, D., 2000, Geophysical exploration for geothermal resources: an application for combined MT-TDEM: Annual Meeting of the Society of Exploration Geophysicists, Calgary, 4 p.

DeLugao, P. P., and Wannamaker, P. E., 1996, Calculating the two-dimensional magnetotelluric Jacobian in finite elements using reciprocity: Geophysical Journal International, v. 127, p. 806–810.

Elders, W. A., Hoagland, J. R., McDowell, S. D., and Cobo, J. M., 1979, Hydrothermal mineral zones in the geothermal reservoir of Cerro Prieto: Geothermics, v. 8, p. 201–209.

Ellis, A. J., and Mahon, W. A. J., 1977, Chemistry and Geothermal Systems: New York, Academic Press, 392 p.

Escher, B. G., 1925, L'eboulement prehistorique de Tasikmalaya et le volcan Galoenggoeng Java: Leidse Geologische Mededelingen , v. 1, p. 8–21.

Davies, R. M., and Ballantyne, G. H., 1987, Geology of the Ladolam deposit, Lihir Island, Papua New Guinea: PACRIM Congress '87, Gold Coast, 1987, Melbourne, Australasian Institute of Mining and Metallurgy, p. 943–949.

Flörke, O. W., Graetsch, H., Martin, B., Roller, K., and Wirth, R., 1991, Nomenclature of micro- and non crystalline silica minerals, based on structure and microstructure: Neues Jahrbuch für Mineralogie Abhandlungen, v. 163, p. 19–42.

Fournier, R. O., 1967, The porphyry copper deposit exposed at Liberty open-pit mine near Ely, Nevada, Part I: Economic Geology, v. 62, p. 57–81.

—— 1981, Application of water geochemistry to geothermal exploration and reservoir Engineering, *in* Rybach, L., and Muffler, L. J. P., editors, Geothermal Systems: Principles and Case Histories: New York, John Wiley and Sons, p. 109–143.

—— 1983, A method of calculating quartz solubilities in aqueous sodium chloride solution: Geochimica et Cosmochimica Acta, v. 47, p. 579–586.

—— 1985, The behavior of silica in hydrothermal solutions, *in* Berger, B. R., and Bethke, P. M., editors, Geology and Geochemistry of Epithermal Systems: Reviews in Economic Geology, v. 2, p. 45–62.

—— 1987, Conceptual models of brine evolution in magmatic-hydrothermal systems, Volcanism in Hawaii: United States Geological Survey Professional Paper 1350, p. 1487–1506.

—— 1999, Hydrothermal processes related to movement of fluid from plastic into brittle rock in the magmatic-epithermal environment: Economic Geology, v. 94, p. 1193–1211.

Fournier, R. O., and Potter, R. W., II, 1982, A revised and expanded silica (quartz) geothermometer: Geothermal Resources Council Bulletin, v. 11, p. 3–12.

Fournier, R. O., and Truesdell, A. H., 1973, An empirical Na-K-Ca geothermometer for natural waters: Geochimica et Cosmochimica Acta, v. 37, p. 1255–1275.

Fujikawa, T., and Ikegami, M., 1992, 110 Mw geothermal power station in Japan - completion of Hatchobaru No. 2 unit: Geothermal Resources Council Transactions, v. 16, p. 561–565.

Giggenbach, W. F., 1984 Mass transfer in hydrothermal alteration systems: a conceptual approach: Geochimica et Cosmochimica Acta, v. 48, p. 2693–2711.

—— 1987, Redox processes governing the chemistry of fumarolic gas discharges from White Island, New Zealand: Applied Geochemistry, v. 2, p. 143–161.

—— 1988, Geothermal solute equilibria. Derivation of Na-K-Mg-Ca geoindicators: Geochimica et Cosmochimica Acta, v. 52, p. 2749–2765.

—— 1991, Chemical techniques in geothermal exploration, *in* D'Amore, F., editor, UNITAR/UNDP Guidebook: Application of Geochemistry in Geothermal Reservoir Development, p. 119–144.

—— 1992, Magma degassing and mineral deposition in hydrothermal systems along convergent plate boundaries: Economic Geology, v. 87, p. 1927–1944.

—— 1993, Redox control of gas compositions in Philippine volcanic-hydrothermal systems: Geothermics, v. 22, no. 5/6, p. 575–587.

—— 1997, The origin and evolution of fluids in magmatic-hydrothermal systems, *in* Barnes, H. L., editor, Geochemistry of Hydrothermal ore deposits: New York, John Wiley and Sons, p. 737–789.

Giggenbach, W. F., and Goguel, R. L., 1989, Collection and analysis of geothermal and volcanic water and gas discharges: Petone, New Zealand, Department of Scientific and Industrial Research Report CD 2401, 4th edition.

Gíslason, S. R., Heaney, P. J., Oelkers, E. H., and Schott, J., 1997, Kinetic and thermodynamic properties of moganite, a novel silica polymorph: Geochimica et Cosmochimica Acta, v. 61, p. 1193–1204.

Goldstein, R. H., and Reynolds, T. J., 1994, Systematics of Fluid Inclusions in Diagenetic Minerals: Society for Sedimentary Geology Short Course 31, 199 p.

Gonzalez, R. C., Alcobar, E. H., Siega, F. L., Saw, V. S., Maximo, D. A., Ogena, M. S., Sarmiento, Z. F., and Guillen, H. V., 2005, Field management strategies for the 700 Mw Greater Tongonan geothermal field, Leyete, Philippines: Proceedings World Geothermal Congress 2005, Antalya, Turkey, 9 p.

Grant, M., Donaldson, I. G., and Bixley, P. F., 1982, Geothermal Reservoir Engineering: New York, Academic Press, 369 p.

Haas, J. L., 1971, The effect of salinity on the maximum thermal gradient of a hydrothermal system at hydrostatic pressure: Economic Geology, v. 66, p. 940–946.

Hadi, J., Harrison, C., Keller, J., and Rejeki, S., 2005, Overview of the Darajat reservoir characterization: a volcanic hosted reservoir: Antalya, Turkey, Proceedings World Geothermal Conference 2005, 11 p.

Hayba, D. O., Bethke, P. M., Heald, P., and Foley, N. K., 1985, Geologic, mineralogic, and geochemical characteristics of volcanic-hosted epithermal-metal deposits, *in* Berger, B. R., and Bethke, P. M., editors, Geology and Geochemistry of Epithermal Systems: Reviews in Economic Geology, v. 2, p. 129–167.

Hanano, M., and Matsuo, G., 1990, Initial state of the Matsukawa geothermal reservoir: reconstruction of a reservoir pressure profile and its implications: Geothermics, v. 19, p. 541–560.

Heaney, P. J., and Post, J. E., 1992, The widespread distribution of a novel silica polymorph in microcrystalline quartz varieties: Science, v. 255, p. 441–443.

Hedenquist, J. W., 1990, The thermal and geochemical structure of the Broadlands-Ohaaki geothermal system, New Zealand: Geothermics, v. 19, p. 151–185.

—— 1995, The ascent of magmatic fluid: discharge versus mineralization *in* Thompson, J. H. F., editor, Magmas, Fluids and Ore Deposits: Mineralogical Association of Canada Short Course Series, v. 23, p. 263–289.

—— 1998, The ascent of magmatic fluid: discharge versus mineralization, *in* Thompson, J. F. H., editor, Magmas, Fluids, and Ore Deposits: Mineralogical Association of Canada Short Course Series, v. 23, p. 263–289.

Hedenquist, J. W., and Henley, R. W., 1985, The importance of CO_2 on freezing point measurements of fluid inclusions: evidence from active geothermal systems and implications for epithermal ore deposition: Economic Geology, v. 80, p. 1379–1406.

Hedenquist, J. W., Reyes, A. G., Simmons, S. F., and Taguchi, S., 1992, The thermal and geochemical structure of geothermal and epithermal systems; A framework for interpreting fluid inclusion data: European Journal of Mineralogy, v. 4, p. 989–1015.

Hedenquist, J. W., Matsuhisa, Y., Izawa, E., White, N. C., Giggenbach, W. F., and Aoki, M., 1994, Geology, geochemistry, and origin of high sulfidation Cu-Au mineralization in the Nansatsu District, Japan: Economic Geology, v. 89, p. 1–30.

Hedenquist, J. W., Arribas, A., and Reynolds, T. J., 1999, Evolution of an intrusion-centered hydrothermal

system: Far Southeast-Lepanto porphyry and epithermal Cu-Au deposits, Philippines: Economic Geology, v. 93, p. 373–404.

Hemley, J. J., Hostetler, P. B., Gude, A. J., and Mountjoy, W. T., 1969, Some stability relations of alunite: Economic Geology, v. 64, p. 599–612.

Hemley, J. J., Montoya, J. W., Marinenko, J. W., and Luce, R. W., 1980, Equilibria in the system Al_2O_3-SiO_2-H_2O and some general implications for alteration-mineralization processes: Economic Geology, v. 75, p. 210–228.

Henley, R. W., and Ellis, A. J., 1983, Geothermal systems ancient and modern: A geochemical review: Earth-Science Reviews, v. 19, p. 1–50.

Ingebritsen, S. E., and Sorey, M. L., 1988, Vapor-dominated zones within hydrothermal systems: evolution and natural state: Journal of Geophysical Research, v. 93, p. 13635–13655.

Johnson, J. W., and Lundeen, S. R., 1994, GEMBOCHS thermodynamic data files for use with the EQ3/6 software package: Lawrence Livermore National Laboratory-Yucca Mountain Program Milestone report MOL72, 99 p.

Junghuhn, F., 1853, Java, deszelfs, gedaante, bekleeding en inwendige structuur: Amsterdam, P. N. van Kampen, second edition, 4 volumes.

Kennedy, B. M., and van Soest, M. C., 2006, A helium isotope perspective on the Dixie Valley, Nevada, hydrothermal system: Geothermics, v. 35, p. 26–43.

Kimberly, P., Siebert, L., Luhr, J. F., and Simkin, T., 1998, Volcanoes of Indonesia: Smithsonian Institution: Global Volcanism Program Digital Information Series, GVP-1.

Layman, E. B., and Soemarinda, S., 2003, The Patuha vapour-dominated resource, West Java, Indonesia: Stanford, California, Stanford University, Proceedings of the 28th Workshop on Geothermal Reservoir Engineering, p. 56–65.

Leach, T. M., Wood, C. P., and Reyes, A. G., 1983, Geology and hydrothermal alteration of the Tongonan geothermal field, Leyte, Republic of the Philippines: Miasa, Japan, 4th International Symposium on Water Rock Interaction, p. 275–278.

Mahon, W. A. J., Klyen, L. E., and Rhode, M., 1980, Natural sodium-bicarbonate-sulphate hot waters in geothermal systems: Chinetsu (Journal of the Japan Geothermal Energy Association), v. 17, p. 11–24.

Moore, J. N., and Gunderson, R. P., 1995, Fluid inclusion and isotopic systematics of an evolving magmatic-hydrothermal system: Geochimica et Cosmochimica Acta, v. 59, p. 3887–3907.

Moore, J. N., Adams, M. C., and Anderson, A. J., 2000a, The fluid-inclusion and mineralogic record of the transition from liquid- to vapor-dominated conditions in The Geysers geothermal system, California: Economic Geology, v. 95, p. 1719–1737.

Moore, J. N., Powell, T. S., Heizler, M. T., and Norman, D. I., 2000b, Mineralization and hydrothermal history of the Tiwi geothermal system, Philippines: Economic Geology, v. 95, p. 1001–1023.

Moore, J. N., Christenson, B., Browne, P. R. L., and Lutz, S. J., 2004a, The mineralogic consequences and behavior of descending acid-sulfate waters: an example from the Karaha - Telaga Bodas geothermal system, Indonesia: Canadian Mineralogist, v. 42, p. 1483–1499.

Moore, J., Bruton, C., and Powell, T., 2004b, Wairakite: A potential indicator of fluid mixing: Geothermal Resources Council Transactions, v. 28, p. 495–498.

Moyle, A. J., Doyle, B. J., Hoogvliet, H., and Ware, A. K., 1990, Ladolam gold deposit, Lihir, Island *in* Hughes, F. E., editor, Geology of the Mineral Deposits of Australia and Papua New Guinea: Melbourne, Australasian Institute of Mining and Metallurgy, v. 2, p. 1793–1805.

Mustopa, E. J., Hisashi, J., Mizunaga, H., and Ushijima, K., 2003, Magnetotelluric exploration of geothermal resources at Takigami area in Japan: Geothermal Resources Council Transactions, v. 27, p. 245–248.

Nemčok, M., Murray, B., Christensen, C., Allis, R., Moore, J. N., and Welker, B., 2003, Optimistic and effective reservoir bottoms: an example from Karaha - Telaga Bodas, Indonesia: Geothermal Resources Council Transactions, v. 27, p. 249–253.

Nemčok, M., Moore, J. N., Allis, R., and McCulloch, J., 2004, Fracture development within a stratovolcano: the Karaha - Telaga Bodas geothermal field, Java volcanic arc, *in* Engelder, T., and Cosgrove, J., editors, The Initiation, Propagation, and Arrest of Joints and Other Fractures: London, Geological Society Special Publication, v. 231, p. 223–242.

Nemčok, M., Moore, J. N., Christensen, C., Allis, R., Powell, T., Murray, B., and Nash, G., 2006, Controls on the Karaha - Telaga Bodas geothermal reservoir, Indonesia: Geothermics, v. 36, p. 9–46.

Nesbitt, B. E., 1993, Electrical resistivities of crustal fluids: Journal of Geophysical Research, v. 98, p. 4301–4310.

Oakes, C. S., Bodnar, R. J., and Simonson, J. M., 1990, The system NaCl-$CaCl_2$-H_2O. I. The vapor-saturated ice liquidus: Geochimica et Cosmochimica Acta, v. 54, p. 603–610.

Pellerin, L., Johnston, J. M., and Hohmann, G. W., 1996, A numerical evaluation of electromagnetic methods in geothermal exploration: Geophysics, v. 61, p. 121–137.

Powell, T. S., 2000, A review of exploration gas geothermometry: Stanford, California, Stanford University, Proceedings 25th Workshop on Geothermal Reservoir Engineering, p. 206–214.

Reid, M. E., 2004, Massive collapse of volcano edifices triggered by hydrothermal pressurization: Geology, v. 32, p. 373–376.

Reyes, A. G., 1990, Petrology of Philippine geothermal systems and the application of alteration mineralogy to their assessment: Journal of Volcanology and Geothermal Research, v. 43, p. 279–309.

Reyes, A. G., Giggenbach W. F., Saleras, J. R. M., Salonga, N. D., and Vergara, M. C., 1993, Petrology and geochemistry of Alto Peak, a vapor-cored hydrothermal system, Leyte Province, Philippines: Geothermics, v. 22, p. 479–519.

Richard, M. A., 1990, The Puna Geothermal Venture project. Power for the Island of Hawaii: Geothermal Resources Council Transactions, v. 14, part 1, p. 803–808.

Rimstidt, J. D., and Barnes, H. L., 1980, The kinetics of silica-water reactions: Geochimica et Cosmochimica Acta, v. 44, p. 1683–1699.

Roedder, E., 1984, Fluid Inclusions: Reviews in Mineralogy, v. 12, 644 p.

Roedder, E., and Bodnar, R. J., 1980, Geologic pressure determinations from fluid inclusion studies: Annual Reviews in Earth and Planetary Sciences, v. 8, p. 263–301.

Salonga, N. D., Herras, E. B., Siega, F. L., Seastres, J. S., Jr., and Dacillo, D. B., 2004, Geochemical signatures of the field-wide expansion process of the upper steam zone in Tongonan geothermal field, Philippines *in* Ogena, M., Salonga, N., Stimac, J., and Moore, J., editors, Philippine Geothermal Systems: Response to Production: Geothermics, v. 33, p. 109–142.

Sanders, M. V., and Black, J. E., 1988, Crystallization and recrystallization of growth-zoned vein quartz crystals from epithermal systems-implications for fluid inclusion studies: Economic Geology, v. 83, p. 1052–1060.

Shimada, K., and Fujino, T., 1995, Deep-seated geothermal resources in Kyushu Island, Japan: Geothermal Resources Council Transactions, v. 19, p. 365-376.

Shinohara, H., 1994, Exsolution of immiscible vapor and liquid phases from a crystallizing silicate melt: Implications for chlorine and metal transport: Geochimica et Cosmochimica Acta, v. 58, p. 5215–5221.

Simmons, S. F., and Browne P. R. L., 1997, Saline fluid inclusions in sphalerite from the Broadlands - Ohaaki geothermal system: A coincidental trapping of fluids being boiled toward dryness: Economic Geology, v. 92, p. 485–489.

Simmons, S. F., Arehart, G., Simpson, M. P., and Mauk, J. L., 2000, Origin of massive calcite veins in the Golden Cross low sulfidation, epithermal Au-Ag deposit, New Zealand: Economic Geology, v. 95, p. 99–112.

Sterner, S. M., Hall, D. L., and Bodnar, R. J., 1988, Synthetic fluid inclusions. V. Solubility relations in the system NaCl-KCl-H_2O under vapor-saturated conditions: Geochimica et Cosmochimica Acta, v. 52, p. 989–1005.

Stimac, J., Moore, J., and Latayan, J., 2006, Hydrothermal alteration and evolution of the Bulalo geothermal field, Philippines: Geothermal Resources Council Transactions, v. 30, p. 959–964.

Stoffregen, R. E., 1987, Genesis of acid-sulfate alteration and Au-Cu-Ag mineralization at Summitville, Colorado: Economic Geology, v. 82, p. 1575–1591.

Suryadarma, Azimuddin, T., Dwikorianto, T., and Fauzi, A., 2005, The Kamojang geothermal field: Antalya, Turkey, Proceedings World Geothermal Congress 2005, 5 p.

Tamanyu, S., and Fujimoto, K., 2005, Hydrothermal and heat source model for the Kakkonda geothermal field, Japan: Proceedings World Geothermal Congress 2005, Antalya, Turkey, 5 p.

Tarantola, A., 1987, Inverse Problem Theory: New York, Elsevier, 671 p.

Torgerson, T., Lupton, J. E., Sheppard, D. S., and Giggenbach, W. F., 1982, Helium isotope variations in the thermal areas of New Zealand: Journal of Volcanology and Geothermal Research, v. 12, p. 283–298.

Tripp, A., Moore, J., Usher, G., and McCulloch, J., 2002, Gravity modeling of the Karaha - Telaga Bodas geothermal system, Indonesia: Stanford, California, Stanford University, Proceedings 27th Workshop on Geothermal Reservoir Engineering, p. 444–452.

Truesdell, A. H., and Singers, W., 1974, The calculation of aquifer chemistry in hot-water geothermal systems: Journal of Research of the United States Geological Survey, v. 2, no. 3, p. 271–278.

Truesdell, A. H., and White, D. E., 1973, Production of superheated steam from vapor-dominated geothermal reservoirs: Geothermics, v. 2, p. 154–173.

Uchida, T., 2003, Application of 3D inversion to magnetotelluric data in the Ogiri geothermal area, Japan: Geothermal Resources Council Transactions, v. 27, p. 245–248.

——— Three-dimensional magnetotelluric investigation in geothermal fields in Japan and Indonesia: Antalya, Turkey, Proceedings World Geothermal Congress 2005, 12 Ucp.

Uchida, T., Lee, T. J., Sasaki, Y., Honda, M., and Andan, A., 2001, 3-D interpretation of magnetotelluric data at the Bajawa geothermal field, Indonesia: Geothermal Resources Council Transactions, v. 25, p. 433–438.

Uchida, T., Lee, T. J., and Cerv, V., 2003, 3-D inversion of magnetotelluric data in the Kakkonda geothermal field, northern Japan: Proceedings 6th Society of Exploration Geophysicists of Japan International Symposium, p. 274–280.

Ussher, G., Harvey, C., Johnston, R., and Anderson, E., 2000, Understanding the resistivities observed in geothermal systems: Beppu, Japan, Proceedings World Geothermal Congress, p. 1915–1920.

Ward, S. H., Parry, W. T., Nash, W. P., Sill, W. R., Cook, K. L., Smith, R. B., Chapman, D. S., Brown, F. H., Whelan, J. A., and Bowman, J. R., 1978, A summary of the geology, geochemistry and geophysics of the Roosevelt Hot Springs thermal area, Utah: Geophysics, v. 43, p. 1515–1542.

Wannamaker, P. E., 1999, Affordable magnetotellurics: interpretation in natural environments, *in* Oristaglio M., and Spies, B., editors, Three-dimensional electromagnetics: Society of Exploration Geophysics, Geophysical Development Series, v. 7, p. 349–374.

Wannamaker, P. E., Doerner, W. M., Stodt, J. A., and Johnston, J. M., 1997, Subdued state of tectonism of the Great Basin interior relative to its eastern margin based on deep resistivity structure: Earth and Planetary Science Letters, v. 150, p. 41–53.

Wannamaker, P. E., Raharjo, I., Moore, J. N., and Allis, R., 2004, Magnetotelluric resistivity section and physical implications through the Telaga Bodas magmatic geothermal system, Indonesia: Geothermal Resources Council Transactions, v. 28, p. 369–371.

White, D., Muffler, L. P. J., and Truesdell, A. H., 1971, Vapor-dominated hydrothermal systems compared with hot-water systems: Economic Geology, v. 66, p. 75–97.